Biol Cybern (2006) 94: 67–85
DOI 10.1007/s00422-005-0032-x

REVIEW

Biological Cybernetics

Sietse M. van Netten

Hydrodynamic detection by cupulae in a lateral line canal: functional relations between physics and physiology

Received: 16 October 2004 / Accepted: 18 October 2005 / Published online: 29 November 2005

Abstract In the present review, signal-processing capabilities of the canal lateral line organ imposed by its peripheral architecture are quantified in terms of a limited set of measurable physical parameters. It is demonstrated that cupulae in the lateral line canal organ can only partly be described as canal fluid velocity detectors. Deviation from velocity detection may result from resonance, and can be characterized by the extent to which a single dimensionless resonance number, N_r, exceeds 1. This number depends on four physical parameters: it is proportional to cupular size, cupular sliding stiffness and canal fluid density, and inversely proportional to the square of fluid viscosity. Situated in a canal, a cupula may benefit from its resonance by compensating for the limited frequency range of water motion that is efficiently transferred into the lateral line canal. The peripheral transfer of hydrodynamic signals, via canal and cupula, leads to a nearly constant sensitivity to outside water acceleration in a bandwidth that ranges from d.c. to a cut-off frequency of up to several hundreds of Hertz, significantly exceeding the cut-off frequency of the lateral line canal. Threshold values of hydrodynamic detection by the canal lateral line organ are derived in terms of water displacement, water velocity, water acceleration and water pressure gradients and are shown to be close to the detection limits imposed by hair cell mechano-transduction in combination with the physical constraints of peripheral lateral line signal transfer. The notion that the combination of canal- and cupular hydrodynamics effectively provides the lateral line canal organ with a constant sensitivity to water acceleration at low frequencies so that it consequently functions as a low-pass detector of pressure gradients, supports the appropriateness of describing it as a sense organ that "feels at a distance" (Dijkgraaf in Biol Rev 38:51–105, 1963).

Sietse M. van Netten
Department of Neurobiophysics, University of Groningen,
Nijenborgh 4, 9747 AG Groningen, The Netherlands
Tel.: +31 50 3634741
Fax: +31 50 3634740
E-mail: s.van.netten@phys.rug.nl

1 Introduction

Most aquatic vertebrates possess a mechano-sensitive lateral line organ (for reviews see Dijkgraaf 1963; Bleckmann 1993; Coombs and Montgomery 1999). This sense organ, which, like the inner ear, is part of the acoustico-lateralis system, enables fishes and amphibians to detect small mechanical disturbances in the water close to the animal. The related sense has been described as the capacity to "feel at a distance" (Dijkgraaf 1963; e.g. Coombs and Montgomery 1999) and operates at frequencies from d.c. up to hundreds of Hertz.

The lateral line organ is instrumental in a diversity of tasks ranging from the detection of local near field water motion (e.g. Harris and van Bergeijk 1962), such as for instance produced by prey (Bleckmann 1980; Elepfandt 1982; Hoekstra and Janssen 1985; Montgomery and Macdonald 1987; Enger et al. 1989) or predator (e.g. Bleckmann 1993) or during schooling (Partridge and Pitcher 1980), to the perception of static obstacles via the detection of the disturbance in the animal's own generated flow field (Hassan 1986; Abdel-Latif et al. 1990). Recently, also a role in rheotaxis has been reported (Montgomery et al. 1997).

The significance of the lateral line system for the detection of water motion was first described by Leydig (1850). He investigated the subsystem of canal lateral line organs, in which the functional mechano-detecting elements, called neuromasts, are located in canals recessed in the skin epidermis of fish (Fig. 1a). The lateral line organ owes its name to this subsystem because of the marked longitudinal appearance of canals along the trunk of several fish species. About one decade later, Schulze (1861) recognized the detection of fluid motion by the units belonging to the other main subsystem, called free or superficial neuromasts. These units, found in both fishes and aquatic amphibians, are positioned on the animal's skin surface from which they project into the surrounding water (Fig. 1b). Much information on the mechano-sensory lateral line system has since been obtained in studies regarding morphological and physiological aspects and behavioral responses mediated by the system (e.g. Dijkgraaf

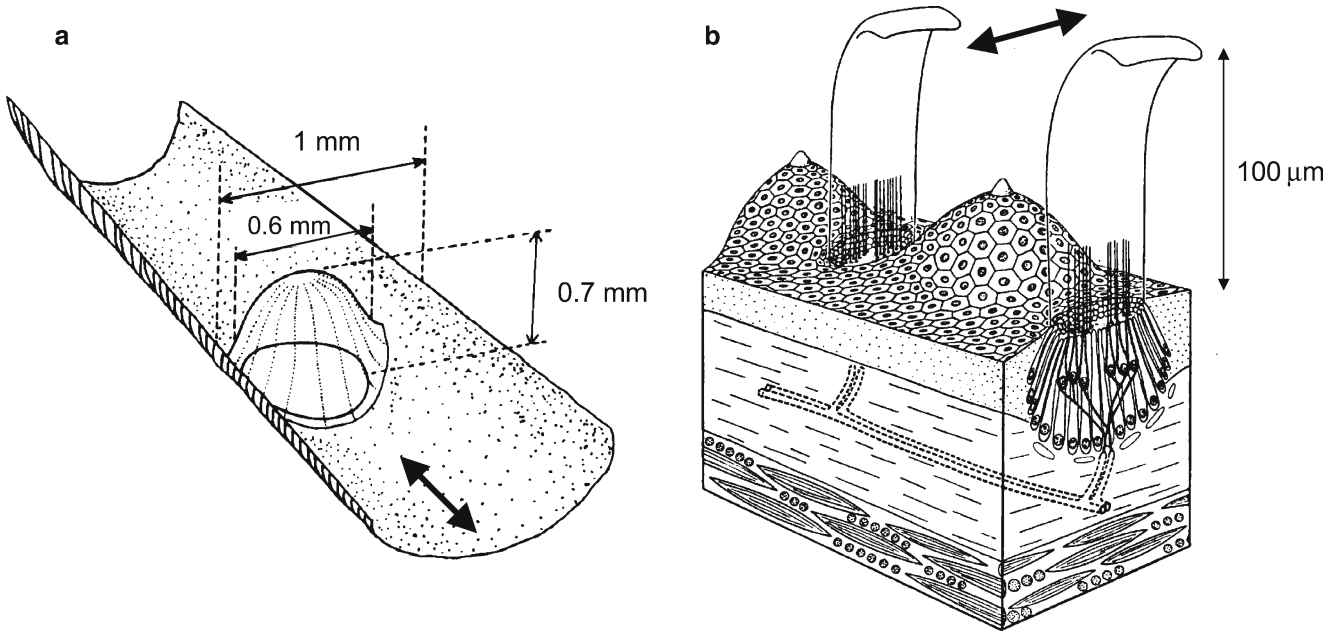

Fig. 1 Schematics of **a** lateral line neuromast in a canal in the absence of the skin and bone that normally covers the canal. Dimensions indicated are typical for the supraorbital canal of ruffe (*Gemnocephalus cernuus*; after van Netten 1991). **b** Schematics superficial neuromasts of the clawed frog (*Xenopus laevis*; after Görner 1963). The *thick arrows* indicate the direction of mechano-sensitivity of both types of lateral line neuromasts, which is related to the directional sensitivity of the hair cells

1963; Cahn 1967; Coombs et al. 1989; Bleckmann 1993; Coombs and Montgomery 1999).

In both the canal- and superficial lateral line organs, a neuromast consists of a cupula overlying a number of sensory hair cells, projecting their mechano-sensitive organelle, a staircase-like hair bundle, into the cupular base. Hair cell numbers vary greatly, but in general canal neuromasts possess hundreds to thousands, whereas superficial neuromasts contain typically tens of hair cells. Hair cells are the primary mechano-transducer cells and transform their bundle's motion into an electrical signal (reviewed by Hudspeth et al. 2000). The transduction sensitivity is selectively polarized along the direction of the bundle's staircase (e.g. Flock 1965), which is either along the direction of the canal (arrow, Fig. 1a; canal neuromast) or parallel to the cupular long cross-sectional axis (arrow, Fig. 1b; superficial neuromast). The transduced signal, encoded in action potentials, is passed on to the brain. Cupular motion, resulting in a motion of the hair bundles in their mechano-sensitive direction, therefore, represents an important stage in the signal-processing cascade of the lateral line organ.

Obviously, cupular motion is induced by the hydrodynamic fluid forces produced by the fluid that flows past the cupula. Since this fluid force is commonly assumed to be of a viscous nature, an elastically coupled cupula is usually described as being displaced in proportion to the relative velocity of the excitatory fluid flow, effectively rendering the cupula a fluid velocity detector. Studies based on electrophysiological recordings supported this model of drag-excitation of the cupula to different extents (Jielof et al. 1952; Görner 1963; Strelioff and Honrubia 1978; Kroese et al. 1978; Kroese and van den Bercken 1982; Denton and Gray 1983; Kroese and Schellart 1992).

Some of these studies suggested that the superficial- and canal lateral line subsystems are not only morphologically distinct, but also differ functionally in their detection character. On the basis of the rate and phase of afferent action potentials generated by superficial neuromasts, these units were described as detectors of the velocity of fluid, whereas canal neuromasts rather detect the surrounding fluid's acceleration (Coombs and Janssen 1990; Kroese and Schellart 1992; Engelmann et al. 2000). The notion that canal neuromasts detect the acceleration of the fluid around an animal could be reconciled to considering canal cupulae as detectors of velocity of the fluid in the canal, as this velocity appeared to be proportional to the acceleration of the water outside the fish at low frequencies (Denton and Gray 1983, 1988, 1989; Kalmijn 1989).

Most evidence on the physical detection characteristics of the peripheral lateral line system has been obtained from recordings of afferent nerve activity. Direct measurements of cupular displacement in response to hydrodynamic stimuli, with the aim to independently test the drag-excitation hypothesis, have been performed in a limited number of studies and on only a few species. Such measurements, performed in the micrometer range using optical microscopy (Jielof et al. 1952; Kuiper 1956; Liff and Shamres 1972; Denton and Gray 1989), suggested a more complicated behavior than that predicted from the drag-excitation hypothesis, some indicating resonance behavior and others excitation resulting from a more complicated fluid boundary layer.

Cupular- and canal fluid dynamics have been determined with nanometer accuracy using laser interferometric techniques (van Netten and Kroese 1987, 1989; van Netten 1988; van Netten and Khanna 1994; van Netten and van Maarseveen 1994; Tsang and van Netten 1997; Wiersinga-Post and van Netten 2000; Ćurčić-Blake and van Netten 2005). Mechano-physiological and theoretical studies (van Netten and Kroese 1989; van Netten 1991; Wiersinga-Post and van Netten 2000) revealed that especially for the case of relatively large cupulae situated in wide lateral line canals, the fluid forces acting on the cupular surface arise from a frequency-dependent boundary layer. Because of changes in its thickness the dominant fluid force on the cupula changes its character from viscous to inertial as frequency increases in the physiological relevant range (d.c. to hundreds of Hertz). Depending on the elastic connections to the canal wall and its dimensions, a cupula may also show resonance behavior. This may lead to a more complicated detection behavior of a cupula than just velocity sensitivity and therefore violates the drag-excitation hypothesis.

In the present review, I will address how the properties of the fluid–cupula-hair cell interactions affect the transfer of hydrodynamic signals by the peripheral lateral line system. Based on previous work, it will be shown that the physical parameters of a lateral line neuromast combine to a dimensionless number, now termed the resonance number, N_r. This number characterizes whether a neuromast can be considered a velocity detector or to what extent its detection characteristics deviate from this because of resonance properties.

As opposed to superficial neuromasts, those situated in the lateral line canal receive their stimuli via the fluid flow in the canal, which is a filtered version of the water flow outside the fish. It will be demonstrated how the combination of canal filtering and cupular resonance can nevertheless be balanced so as to ensure an essentially frequency independent transfer of local hydrodynamic stimuli to the mechano-detecting hair cells, at frequencies up to hundreds of Hertz.

The approach taken here specifically focuses on how the physical parameters of the peripheral lateral line organ govern the physiological detection characteristics and capabilities of the organ. It may thus serve as a basis for a quantitative investigation of the relationship between morphological diversity of the lateral line system (Webb 1989; Münz 1989; Coombs et al. 1988; Northcutt 1989) and its consequences for the possible diversity in hydrodynamic field detection.

2 Hydrodynamics and mechanics of cupular excitation

2.1 Experimental determination of cupular displacement in response to canal fluid displacement

Hydrodynamic signals encoded in the local water flow around an animal are transferred to a lateral line neuromast via the fluid forces that act on the cupula, resulting in its displacement. Figure 2 shows representative examples of laser-interfer ometrically measured displacements of supra-orbital canal

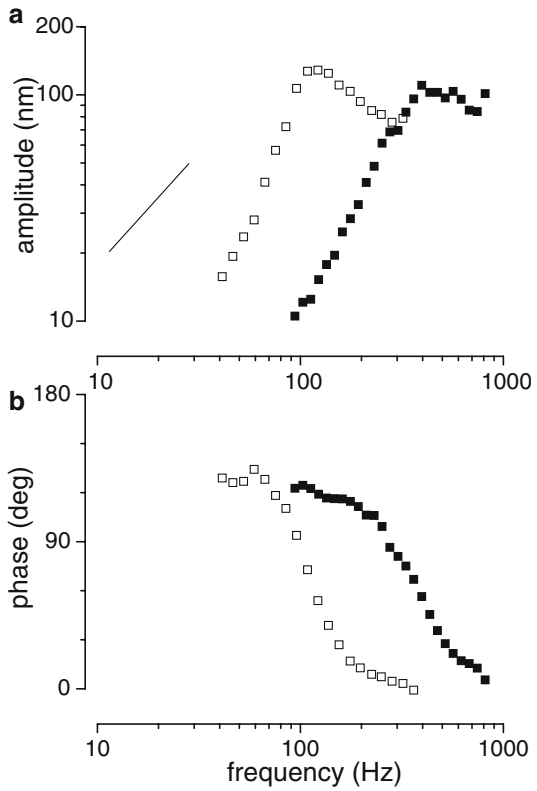

Fig. 2 Cupular displacement amplitude (**a**) and phase (**b**) measured using laser interferometry in the ruffe (*open symbols*) and the African knife fish (*closed symbols*) in response to fluid vibrations in the canal produced with a sphere (Ø ≠ 0.8 mm) with constant displacement amplitude of the order of 1 μm (Wiersinga-Post and van Netten 2000). The *solid line* (**a**) indicates a slope of 20 dB/decade, which is expected for pure velocity detectors. The phase of cupular displacement shown (**b**) is referred to the phase of the displacement stimulus sphere

cupulae of the ruffe (*Acerina cernua* or *Gymnocephalus cernuus*, open squares) and the African knife fish (*Xenomystis nigri*, filled squares). These cupular displacements were measured in response to a vibrating stimulus sphere placed in the canal at a distance of a few millimeters from the cupula (Wiersinga-Post and van Netten 2000). At such distances the fluid displacement produced in the canal is proportional and in phase with that of the sphere (Tsang and van Netten 1997). The stimulating sphere's displacement amplitude was kept constant so that cupular motion in the physiologically relevant displacement range ($< 1\ \mu$m) was evoked, while its vibrational frequency was varied.

Figure 2 shows that the effective filter characteristics resulting from the fluid–cupula interaction is similar for both types of neuromasts, except for an upward frequency-shift of the African knife fish's response as compared to that of the ruffe. The transfer of low frequency fluid displacements to displacement of the cupula is clearly suppressed. The amplitude of cupular displacement increases with (low) frequency along slopes that are steeper than 20 dB/decade (Fig 2a, cf. solid line), until a maximum is reached at about 120 Hz for the ruffe

and at about 400 Hz for the African knife fish. At frequencies beyond these resonance frequencies, cupular displacement tends to decrease to a constant value.

The measured cupular phase with respect to the phase of the excitatory canal fluid displacement is in line with its amplitude characteristics. The cupular phase lead, which exceeds 90° at low frequencies, declines most steeply around the resonance frequencies. Also, a phase lead approaching zero is consistent with a constant displacement amplitude at frequencies beyond resonance, indicating that a cupula directly follows the displacement of the excitatory fluid at high frequencies. Cupular motion at the apex was found to equal that of its base indicating that the canal cupula moves without significant bending under physiological stimulus conditions (van Netten and Kroese 1987).

The frequency responses measured can only be partly explained by the filtering properties of a second order fluid driven- and damped mass-stiffness system as proposed in studies of cupular mechanics (Kuiper 1956; Kalmijn 1988). In the next sections a more detailed model of cupular excitation (van Netten 1991) will be considered.

2.2 Theory of excitatory fluid forces

To determine the fluid forces acting on a cupula by a vibrating fluid, first the forces are considered that are required to vibrate a cupula in a fluid, which is at rest at large distances. To calculate these fluid forces, the shape of the cupula is approximated by a sphere.

Because the (non-steady) velocities of fluid and cupula under physiological conditions, as well as the ratio of (maximal) characteristic lateral line dimensions (< 0.1 m) and shortest times (~ 1 ms) relevant to the system (e.g. van Netten 1991, Sect. 2.6) are well below the velocity of underwater sound (~ 1440 m/s), the fluid may be considered to be incompressible (e.g. Landau and Lifshitz 1987). This implies that the compression related component of the fluid flow, usually referred to as the far field, can be neglected and that the near field remains as the main fluid flow component that directly stimulates the lateral line system [e.g. Harris and van Bergeijk 1962; see also Sect. A.1 (Appendix)]. In certain fish, adaptations to the hearing - and lateral line organ cause external pressure changes to be transformed into lateral line fluid displacement (Denton and Blaxter 1976), for which incompressibility can also be assumed.

Another important simplification on lateral line hydrodynamics concerns its linearization. For periodic motion produced by a solid body this is justified (Landau and Lifshitz 1987), if the vibratory displacement amplitude of fluid flow, usually no more than the order of 1 μm, is much smaller than the dimensions of the body itself, a condition that is amply met for the neuromasts that will be considered here, which have typical dimensions of fractions of 1 mm.

Under these simplifications of an effective incompressible and linear fluid, Stokes (1851) derived a mathematical solution of the near field flow pressure, (p) and velocity ($\mathbf{v}$) generated by a rigid sphere with radius (a) and vibrating with angular frequency (ω) in a fluid with viscosity μ and density ρ, by solving the accordingly simplified Navier–Stokes equation:

$$\rho\left(\frac{\partial \mathbf{v}}{\partial t}\right) + \nabla p - \mu\nabla^2\mathbf{v} = 0, \tag{1}$$

in combination with the equation of continuity for an incompressible fluid:

$$\nabla\mathbf{v} = 0. \tag{2}$$

The center position of the oscillating sphere will be denoted by $X(t) = B\sin(\omega t)$, which, therefore, also prescribes the motion of the fluid at the sphere's surface. In line with the assumption above of linear flow, the amplitude, (B), has to be small compared to the sphere's radius, a (i.e. $B << a$). This assumption allows that the position of the sphere's vibrating surface at which the fluid flow is described, can be treated as a fixed boundary (Stokes 1851).

The calculated flow field as generated by the vibrating sphere under these conditions is symmetrical around the axis of vibration and in spherical coordinates (r is distance to the sphere's center; θ is the angle with the axis of vibration), the pressure, $p(r, \theta)$, is (Stokes 1851, e.g. Lamb 1932):

$$p(r,\theta) = -\frac{\rho a^3 B\omega^2}{2r^2}\cos\theta\left[C_1(\delta, a)\sin\omega t - C_2(\delta, a)\cos\omega t\right], \tag{3}$$

where the boundary layer thickness around the sphere (δ), is given by:

$$\delta(\omega) = \sqrt{\frac{2\mu}{\rho\omega}}, \tag{4}$$

while the functions C_1 and C_2 depend on the ratio of sphere radius to the boundary layer thickness according to:

$$C_1(\delta, a) = 1 + \frac{3\delta(\omega)}{2a} \tag{5}$$

and

$$C_2(\delta, a) = \frac{3\delta(\omega)}{2a}\left[1 + \frac{\delta(\omega)}{a}\right]. \tag{6}$$

Integrating the pressure and shear stress components in the direction of the sphere's motion over its entire surface (cf. Landau and Lifshitz 1987, p 60), amounts to (Stokes 1851; Lamb 1931; Landau and Lifshitz 1987, cf. van Netten 1991):

$$F_{\text{fluid}}(\omega) = -6\pi a\mu B\omega\left[\left(1 + \frac{a}{\delta(\omega)}\right)\cos(\omega t) - \frac{a}{\delta(\omega)}\left(1 + \frac{2a}{9\delta(\omega)}\right)\sin(\omega t)\right]. \tag{7}$$

The first term within square brackets of the right-hand side of (7) represents the viscous fluid force on the sphere, which is in anti-phase with its velocity ($dX/dt = B\omega\cos(\omega t)$). At low frequencies (i.e. if $\delta >> a$, cf. Eq. 4) this term dominates the fluid force so that it approaches the familiar result

known as Stokes' law: $F_{\text{fluid}} = -6\pi\, a\mu \cdot dX/dt$. The second term between square brackets, which is in anti-phase with the acceleration of the sphere ($d^2X/dt^2 = -B\omega^2 \sin(\omega t)$; note that $1/\delta^2(\omega) \propto \omega$), and therefore 90° out of phase with the viscous force, represents the inertial fluid force. This term dominates at high frequencies (i.e. if $\delta << a$, cf. Eq. 4), and then approaches the force needed to vibrate half of the fluid mass displaced by the sphere.

For further use in the equation of motion of the cupula it is convenient to convert (7) to complex notation in which sphere displacement is denoted as $X(t) = B\exp(i\omega t)$, so that the sphere's velocity is $dX(t)/dt = i\omega X(t)$. The complex amplitude of the fluid force (7) can then accordingly be expressed as a frequency dependent drag, $[D(\omega)]$, times the velocity, (dX/dt):

$$F_{\text{fluid}}(\omega) = D(\omega)\frac{dX}{dt} = -6\pi a\mu \left[\left(1 + \frac{a}{\delta(\omega)}\right) + i\frac{a}{\delta(\omega)}\left(1 + \frac{2a}{9\delta(\omega)}\right)\right]\frac{dX}{dt} \quad (8)$$

The related radial and tangential fluid velocity components, $v_r(r,\theta)$ and $v_\theta(r,\theta)$, including those within the region of the viscous boundary layer, can also be derived from the work of Stokes (1931) and may be of practical use in the generation of stimuli to the lateral line organ. These are discussed in Sect. A.2 (Appendix).

2.3 Frequency selectivity of cupular sensitivity

The results of the previous section can be utilized to determine the steady-state oscillatory displacement, $Y(t) = Y_0 \exp(i\omega t)$, of a (hemi-)spherical cupula as it is evoked by an oscillating fluid flowing past it which has a displacement, $W(t) = W_0 \exp(i\omega t)$. The force exerted by the fluid on the cupula then equals the drag, $D\ (\omega)$ (e.g. 8), multiplied by the relative velocity between cupula and excitatory fluid, $dY(t)/dt - dW/dt$. In addition to this external fluid force, it is assumed that the cupula is also subject to the force resulting from its elastic coupling to the canal wall which is proportional to the cupular sliding stiffness, K (van Netten and Kroese 1987). This stiffness force can be attributed to the elastic hair bundles of the underlying hair cells, which couple the cupular base (e.g. Fig. 1) to the canal wall (van Netten and Khanna 1994). The equation of motion of cupular displacement, $[Y(t)]$, in response to a fluid displacement $W(t)$ can then be written as:

$$M\ddot{Y}(t) = -KY(t) + D\left[\dot{Y}(t) - \dot{W}(t)\right] + M\ddot{W}(t). \quad (9)$$

Here, time derivatives are indicated as usual and $M = \frac{4}{3}\pi a^3\rho$ denotes the cupular mass, which is assumed to possess the same density, ρ, as the excitatory fluid (e.g. Jielof et al. 1952). The left hand side term in (9), representing the cupular mass times its acceleration is set equal to the external forces acting on the cupula, which consist of the stiffness force, which is proportional to the sliding stiffness, K and the fluid forces resulting from the cupular motion, relative to the velocity of the excitatory fluid. Effectively, the cupula is thus both driven and damped by the fluid. The last term of the right-hand side of (9) represents an additional fluid buoyancy force, related to the acceleration of the amount of fluid displaced by the cupula, having a mass, (M), which is equal to that of the cupula, since its density is taken equal to that of water. The equation of motion (9) is linear and can be solved in the frequency domain, so that only steady-state amplitudes need to be considered, thus expressing the complex amplitude of cupular displacement $[Y_0(f)]$ as a function of excitatory frequency $f = \omega/(2\pi)$ and amplitude (W_0) of water displacement. The time dependence of cupular- and water displacement is thus implicitly given by the exponential time factor $\exp(i2\pi ft)$(i.e. $Y(t) = Y_0\exp(i2\pi ft)$and $W(t) = W_0\exp(i2\pi ft)$). The result for displacement amplitude $[Y_0(f)]$ in response to water displacement with amplitude W_0 is then (e.g. van Netten 1991):

$$Y_0(f) = \frac{i\frac{f}{f_t} + \frac{1}{2}\sqrt{2}(i-1)\left(\frac{f}{f_t}\right)^{\frac{3}{2}} - \frac{1}{3}\left(\frac{f}{f_t}\right)^2}{N_r + i\frac{f}{f_t} + \frac{1}{2}\sqrt{2}\,(i-1)\left(\frac{f}{f_t}\right)^{\frac{3}{2}} - \frac{1}{3}\left(\frac{f}{f_t}\right)^2} W_0, \quad (10)$$

and thus shows that the four physical parameters (K, a, μ and ρ) reduce to only two independent parameters given by:

$$f_t = \frac{\mu}{2\pi\rho a^2}, \quad (11)$$

and

$$N_r = \frac{Ka\rho}{6\pi\mu^2}. \quad (12)$$

The transition frequency (f_t) is directly related to the linear a.c. (unsteady) Reynolds number, $(\text{Re}_{ac} = 2\pi f\rho a^2/\mu = f/f_t$(Batchelor 1967) and indicates at which frequencies viscous ($\text{Re}_{ac} < 1$, equivalent to $f < f_t$) or inertial fluid forces ($\text{Re}_{ac} > 1$, equivalent to $f > f_t$) dominate the fluid forces acting on the cupula. The ratio f_t/f is sometimes called Stokes' number. In (10), f_t appears solely in its ratio to the stimulus frequency (f) and its value can thus also be considered as a normalizing scale factor of the frequency.

The number N_r is dimensionless and effectively determines the shape of a curve depicting cupular sensitivity versus log-frequency (cf. van Netten 1991, where N_r was termed cupular parameter P_c). As will be demonstrated below, the value of N_r governs the resonance properties of a cupula and it will accordingly be referred to as resonance number in the following. The further significance and usefulness of the two independent parameters f_t and N_r, which completely govern the cupular sensitivity given by (10), will be described in detail in the following sections.

The solution of the steady-state cupular displacement amplitude, (Y_0), as given in (10) can also be expressed in terms of excitatory fluid velocity

$$V(t) = \frac{dW(t)}{dt} = i2\pi f W_0 \exp(i2\pi ft) = V_0\exp(i2\pi ft),$$

rather than fluid displacement, $W\ (t)$.

If the (complex) cupular sensitivity to velocity $[S(f)]$ is defined as the ratio of (complex) cupular displacement amplitude $[Y_0(f)]$ to excitatory fluid velocity amplitude $[V_0]$ it follows from (10) by substituting $W_0 = V_0/(i2\pi f)$ and subsequently dividing both sides by V_0, that $S(f)$ is given by:

$$S(f) = \frac{Y_0(f)}{V_0} = \frac{1}{2\pi f_t} \frac{1+\frac{1}{2}\sqrt{2}(1+i)\left(\frac{f}{f_t}\right)^{\frac{1}{2}}+\frac{1}{3}i\frac{f}{f_t}}{N_r+i\frac{f}{f_t}-\frac{1}{2}\sqrt{2}\,(1-i)\left(\frac{f}{f_t}\right)^{\frac{3}{2}}-\frac{1}{3}\left(\frac{f}{f_t}\right)^2}. \quad (13)$$

Equation (13) expressing the frequency dependent cupular sensitivity to velocity will be used in the following sections, rather than the equivalent form (10). Both approaches are completely equivalent but the sensitivity defined in (13) illustrates more clearly how the four physical parameters of the peripheral lateral line that we consider, namely strength of sliding stiffness coupling (K), cupular radius (a) and fluid density (ρ) and viscosity (μ), condensed into the two independent parameters, f_t and N_r, control the extent to which the drag-excitation hypothesis is justified.

It should be noted that the frequency characteristics described by both (10) and (13) are different from those of a second order system, which can be represented by a lumped parameter model. In contrast, the spatially distributed action of the fluid considered here, which is both driving and damping the cupula, gives rise to fractional powers of the frequency (f) which in the time domain may lead to fractional derivatives (cf. Landau and Lifshitz 1987).

2.4 Velocity detecting- and resonating cupulae

Given the typical displacement detection range of hair cells in combination with the conditions under which the lateral line organ operates, an appropriate unit of cupular sensitivity, $S(f) = Y_0(f)/V_0$ (13) is nanometer cupular displacement (Y_0) per micrometer/second fluid velocity (V_0). Note that this unit of cupular velocity sensitivity is equivalent to millisecond. The significance of interpreting cupular sensitivity in terms of time will be discussed in more detail in Sect. 2.6.

To what extent and in which frequency range a cupula can be regarded as a detector of fluid velocity (drag-excitation hypothesis), or alternatively, in which frequency range $S(f)$ is a virtually frequency-independent constant, can be appreciated from considering the numerical values of the two independent parameters f_t and N_r and inspection of (13).

It will first be assumed that $N_r << 1$. Equation (13) then shows that at low frequencies a cupula detects velocity with an almost constant sensitivity (S_v), which is given by:

$$S(f) \cong \frac{1}{2\pi f_t N_r} = S_v \qquad (N_r << 1; \text{low} f). \quad (14)$$

A cupula maintains this virtually constant velocity sensitivity (S_v) up to frequencies at which N_r remains the leading term in the right-hand denominator of (13), i.e. if $N_r > f/f_t$. This leads to a bandwidth of almost constant velocity-sensitivity ranging from d.c. to a cut-off frequency (f_c) given by:

$$f_c = f_t N_r. \quad (15)$$

Equation (15) shows that the cut-off frequency (f_c) lies below the transition frequency (f_t) since it is assumed here that N_r is smaller than 1. This implies that in the whole velocity detecting bandwidth (d.c. to f_c) viscous fluid forces, which dominate below f_t (11), are responsible for the excitation of the cupula.

At frequencies exceeding f_c, the amplitude of cupular sensitivity reduces because of the ratio of the leading terms of the numerator ($\propto f$) and denominator ($\propto f^2$) in (13), so that at these frequencies the sensitivity (13) effectively reduces to:

$$S(f) \cong \frac{1}{2\pi f_t} \frac{\frac{1}{3}i\frac{f}{f_t}}{\frac{-1}{3}\left(\frac{f}{f_t}\right)^2} = \frac{1}{i2\pi f}, \qquad (f > f_c), \quad (16)$$

which corresponds to a sensitivity roll-of of 20 dB/decade. An example of the sensitivity of a cupula with resonance number smaller than 1 ($N_r = 0.1$) is depicted in Fig. 3, and shows that the amplitude of the sensitivity (Fig. 3a) can schematically be represented by two intersecting lines, representative for a first-order linear low-pass filter (dotted lines) possessing a constant velocity sensitivity at low frequencies (i.e. low-pass) given by (14) and displaying a roll-off as expressed by (16) beyond the cut-off frequency, f_c (15). The phase of the sensitivity (Fig. 3b), in line with its definition, is referred to the phase of the excitatory fluid velocity, and is accordingly close to zero in the low frequency (low-pass) range while turning to $-90°$ at frequencies beyond cut-off. A cupula with $N_r << 1$ can therefore be considered a pure velocity detector in the bandwidth limited by d.c. and the cut-off frequency f_c, and shows no significant resonance. The hypothesis of drag–excitation of the cupula thus appears to be valid under the condition that $N_r << 1$ and in the restricted frequency range from d.c. up to f_c, and is expressed indeed by (14), as it is equivalent to balancing the (low frequency) fluid drag force to the stiffness related force (i.e.$6\pi a\mu V_0 = KY_0$).

The situation is different for cupulae with $N_r >> 1$, which can be classified as resonating cupulae as illustrated in Fig. 3 for $N_r = 10$ and 100. At low frequencies ($f << f_t$) the cupular sensitivity equals $S_v = 1/(2\pi f_t N_r)$, which is the same constant sensitivity as that of a pure velocity detecting cupula ($N_r << 1$; cf. Eq. 13). However, in contrast to a pure velocity detecting cupula, the sensitivity of a resonating cupula may significantly increase above S_v, if the stimulus frequency (f) exceeds the transition frequency (f_t). This is the result of inertial fluid forces boosting the displacement of the cupula. If ($N_r >> 1$) the cupula thus exhibits resonance behavior and is tuned to a resonance frequency (f_r) of about [see (13) and van Netten 1991]:

$$f_r \cong f_t\sqrt{3N_r}, \qquad (N_r >> 1), \quad (17)$$

The quality factor (Q) of a resonating cupula can be calculated by considering the expression for the Q-factor of a

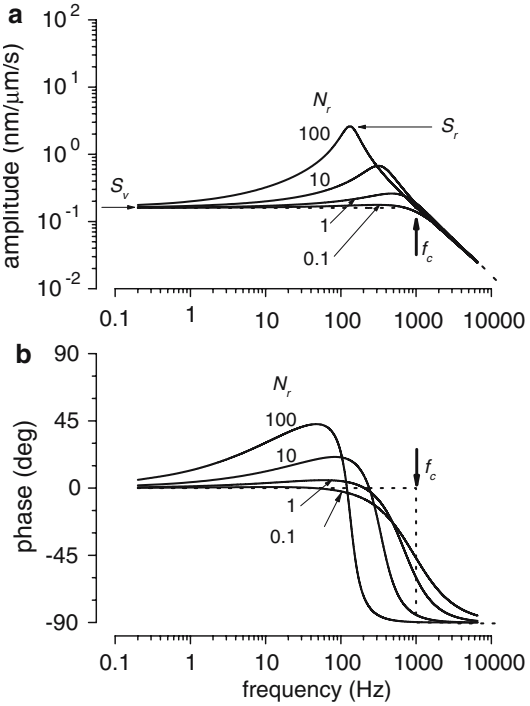

Fig. 3 Effect of resonance number, (N_r), on cupular sensitivity, [$S(f)$], as a function of frequency of vibratory fluid flow in the canal. **a** Amplitude of cupular sensitivity is expressed in nm/(μm/s), which is equivalent to ms. **b**. Phase of cupular sensitivity. The cut-off frequency, $f_\mathrm{c} = f_\mathrm{t} N_\mathrm{r}$, was kept constant (1000 Hz) for all four situations depicted (N_r = 0.1, 1, 10 and 100, as indicated). The low frequency gain, S_v (*left arrow*), is accordingly the same for all four cases depicted. For low N_r numbers (e.g. 0.1) the cupular sensitivity is virtually constant implying that the cupular displacement response is proportional to fluid velocity up to f_c, whereas for high N_r numbers (e.g. 10 and 100) the cupular sensitivity may increase significantly above S_v, due to resonance. The enhanced sensitivity at resonance, S_r, is indicated (*right arrow*) for the case of N_r = 100. An intermediate response results if N_r = 1

second-order damped (D_f), mass (M), stiffness, (K) system ($Q = \sqrt{MK}/D_f$). Although the general responses given by (13) cannot adequately be described by a second-order lumped parameter model, in the restricted frequency range around f_r, assuming $N_\mathrm{r} >> 1$, these responses resemble those of such a resonating second-order system so that the approximation for the Q-factor given above can be used. In that case, D_f is defined by the fluid damping which is frequency dependent and given by the real component of $D(\omega)$ (8). This component approaches $6\pi a\mu\ (a/\delta) = 3\pi a^2\sqrt{2\mu\rho\omega}$ at frequencies around f_r, since its frequency-independent viscous drag-term ($6\pi a\mu$) can then be neglected. This can be derived from the assumption that $N_\mathrm{r} >> 1$ so that with (17) $f_r/f_\mathrm{t} >> 1$, which is equivalent to $a/\delta(\omega) >> 1$ at frequencies around resonance. When evaluated at $\omega = 2\pi f_r$ with f_r, given by (17) the Q- factor then yields:

$$Q \cong \sqrt{\frac{2}{3}} \cdot \left(\frac{N_\mathrm{r}}{3}\right)^{1/4}, \qquad (N_\mathrm{r} >> 1). \tag{18}$$

Equation (18) shows that the cupular Q-factor solely depends on the resonance number (N_r) as expected. This expression is larger by a factor $\sqrt{3/2}(\cong 22\%)$ than an earlier approximation of Q to account for the effective mass of the cupula (M) which because of the entrained fluid is increased by a factor 3/2 (cf. van Netten 1991).

It follows from Eqs. 11, 17 and 15 that the relevant frequencies are mutually related as $f_\mathrm{t} < f_r < f_\mathrm{c}$, when $N_\mathrm{r} >> 1$. Beyond the cut-off frequency, $f_\mathrm{c} = f_\mathrm{t} N_\mathrm{r}$, the amplitude of the sensitivity of a resonating cupula resembles that of a pure velocity detecting cupula and also rolls off with 20 dB/decade, while the phase approaches $-90°$ similar to the behavior of a first-order low-pass filter (see Eq. 16). This is illustrated in Fig. 3, which compares frequency responses of cupulae with N_r smaller and larger than 1, but with the same cut-off frequency ($f_\mathrm{c} = f_\mathrm{t} N_\mathrm{r}$ =1000 Hz). Thus in both types of cupulae, f_c marks the upper range of frequencies of fluid velocity which evoke a cupular motion with a sensitivity of S_v or higher. The effective bandwidth of a cupula with $N_\mathrm{r} >> 1$, however, is smaller than f_c because of the peaked response around resonance (see also Sect. 2.5).

An indication of the order of magnitude of the extra sensitivity, gained by resonance as compared to the low frequency sensitivity (S_v) may be obtained by substituting f_r (17) into (13) and evaluating the remaining leading terms in both the numerator and denominator. The result for the amplitude of cupular sensitivity at resonance, $S_r = |Y_0(f_r)/V_0|$, as compared to the low frequency sensitivity, S_v (14), is then:

$$\frac{S_r}{S_v} \cong \frac{N_r^{3/4}}{3^{5/4}}, \qquad (N_\mathrm{r} >> 1). \tag{19}$$

The ratio of sensitivities in (19) shows that the extra sensitivity at resonance increases almost linearly with the resonance number, N_r. Because of the enhanced sensitivity, a resonating cupula is not exclusively displaced in proportion to fluid velocity but, in a limited range of its bandwidth, from approximately f_t up to f_c, it follows rather a frequency-dependent combination of velocity and acceleration (Fig. 3).

2.5 Application of theory to cupular displacement measurements

The two examples of measured frequency responses of canal lateral line cupulae shown in Fig. 2 were measured in sufficient detail to test the appropriateness of the preceding model description. Figure 4 shows the same measured data as depicted in Fig. 2 but now plotted as cupular sensitivity [$S(f)$] i.e. cupular displacement in the ratio to excitatory fluid velocity rather than displacement, commensurate with the model description (13). In line with relating the data to the excitatory water velocity rather than water displacement, an overall phase lag of 90° has been taken into account in plotting the phase data in Fig. 4b. The solid lines represent the model fits to the data points. From these fits the average values of N_r and f_t of both types of cupulae were determined. Both canal cupulae belong to the resonating class and the similar shape

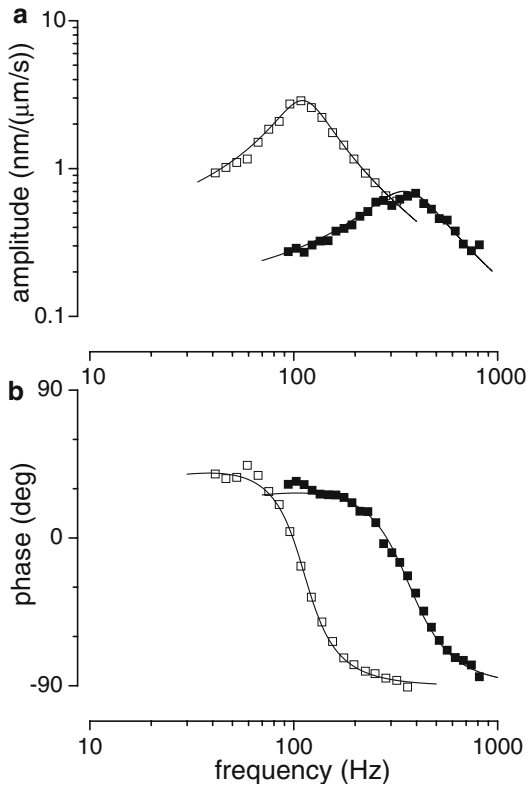

Fig. 4 Same cupular displacement data as shown in Fig. 2 of the ruffe (*open symbols*) and the African knife fish (*closed symbols*), but now shown as cupular sensitivity (13), defined as cupular displacement per canal fluid velocity. **a** Amplitude of sensitivity expressed in nm per μm/s. **b** Phase of sensitivity (90° delayed as compared with Fig. 2b). *Solid lines* show the results of fits (13) to the data points (ruffe: $f_t = 10\,\text{Hz}$, $N_r = 64$; African knife fish: $f_t = 70\,\text{Hz}$, $N_r = 20$)

of the frequency responses is reflected in their similar resonance numbers which as a consequence both significantly exceed one (ruffe: $N_r = 64$; African knife fish $N_r = 20$).

The related quality factors, (ruffe: $Q = 1.74$; African knife fish: $Q = 1.31$; Eq. 18) are rather low, especially in the case of the African knife fish. The transition frequency, f_t (13) of the African knife fish ($f_t = 77\,\text{Hz}$) is a factor of about 7 higher than that of the ruffe ($f_t = 10.6\,\text{Hz}$), primarily because of the former's smaller cupular dimensions (cf. Eq. 13; Wiersinga-Post and van Netten 2000). This results in the relative upward frequency shift of the African knife fish' sensitivity curve. Also, the resonance frequency of the African knife fish cupula ($f_r = 460\,\text{Hz}$) is about a factor 4 higher than that of the ruffe ($f_r = 116\,\text{Hz}$).

The cut-off frequency, $f_c = f_t N_r$, reflects the enhanced related bandwidth of the African knife fish' cupula ($f_c = 1540\,\text{Hz}$) in comparison to that of the ruffe ($f_c = 678\,\text{Hz}$). Note that these cut-off frequencies mark the frequencies at which cupular sensitivity falls below the low frequency sensitivity (S_v) and is theoretically a factor $\sqrt{N_r/3}$ higher than the resonance frequency (f_r). Even these latter frequencies, however, may still be considered an overestimate of the cut-off of the operational frequency range of the lateral line organ, as will be further detailed in Sect. 3.3.

Inversely to the cut-off frequency defined by $f_c = f_t N_r$, the low-frequency cupular sensitivity of the ruffe, $S_v = 0.23\,\text{nm}/(\mu\text{m}\cdot\text{s}^{-1})$ exceeds that of the African knife fish, $S_v = 0.10\,\text{nm}/(\mu\text{m}\cdot\text{s}^{-1})$. The latter value is quite similar to the sensitivity reported for sprat lateral line cupulae ($0.12\,\text{nm}/(\mu\text{m}\cdot\text{s}^{-1})$; Denton and Gray 1989).

2.6 Cupular impulse response and relation to cupular sensitivity

The inverse relationship between cupular sensitivity and detection bandwidth observed in the ruffe's and African knife fish' cupular mechanics (Sect. 2.5) is reminiscent of a more general principle of a fixed sensitivity-bandwidth product. Such a relationship applies to cupular filtering, as follows directly from considering the cupular sensitivity (S_v) defined at low frequencies for both classes of cupulae, in relation to the cut-off frequency f_c (Eqs. 14 and 15), irrespective of N_r:

$$S_v \cdot f_c = \frac{1}{2\pi}. \tag{20}$$

Because of its first-order low-pass filter characteristics, the cut-off frequency (f_c) of a pure velocity detecting cupula ($N_r << 1$) may be taken as the effective cupular filtering bandwidth Δf. Since the time constant (τ) of a first-order low-pass filter is inversely related to its effective bandwidth Δf (i.e. $\tau = 1/(2\pi\,\Delta f)$, Eq. 20 implies an identity between the time constant (τ_v) of the exponentially decaying (velocity) impulse response and the constant sensitivity (S_v) of a pure velocity detecting cupula:

$$\tau_v = \frac{1}{2\pi\,\Delta f} = \frac{1}{2\pi f_c} = S_v, \qquad (N_r << 1). \tag{21}$$

Equation (21) shows that the decay-time constant of a pure velocity detecting cupula, given in milliseconds, equals its cupular sensitivity expressed in nm/(μm/s) (cf. Eq. 14) and accordingly emphasizes the equivalence of units of nm/(μm/s) and ms on the amplitude-axis of the sensitivity curves (e.g. Figs. 3 and 4, see also Sect. 2.4).

A resonating cupula ($N_r >> 1$), on the other hand, has a smaller effective filtering bandwidth than f_c. The narrower bandwidth of the peaked sensitivity of a resonating cupula corresponds in the time domain with an impulse response, which consists of damped oscillations with a frequency of about f_r. The time constant (τ_r) of the envelope of these oscillations can be estimated with the use of the quality factor (Q) and the resonance frequency (f_r) given by (18) and (17). The result is:

$$\tau_r \cong \frac{Q}{\pi\, f_r} \cong 0.72\,\tau_v\, N_r^{3/4} \cong 2\sqrt{2}S_r \qquad (N_r >> 1). \tag{22}$$

Inspecting (22) shows that the transients of the impulse response of a resonating cupula are prolonged in relation to τ_v (21) with a factor, which increases with $N_r^{3/4}$. The same factor was found for the extra sensitivity gained from resonance (19), so that the cupular sensitivity at resonance (S_r) may be

Table 1 Canal lateral line sensitivities and threshold detection levels.

Description	Symbol	Theory	Ruffe
Low frequency cupular velocity sensitivity	$S(0) = S_V$	$\frac{1}{2\pi f_t N_r}$	0.23 nm/(μm/s) (= ms)
Low frequency canal acceleration sensitivity	$S_{can}(0,0)$	$\frac{1}{2\pi f_{can}}$	10 (μm/s)/(mm/s^2) (= ms)
Combined lateral line organ acceleration sensitivity	$S_{llo}(0)$	$S_V \cdot S_{can}$	2.3 – 4 nm/(mm/s^2) (= ms^2)
Hair cell displacement detection threshold	$T_{X,TD}$	$\frac{1}{\sqrt{N_{ch}}}\frac{2kT}{Z}$	6.5 nm *
Neuromast fluid displacement detection threshold	T_X	$\left(\left(\frac{kT}{K}\right) + \frac{1}{N_{ch}N}\left(\frac{2kT}{Z}\right)^2\right)^{\frac{1}{2}}$	0.3 – 2.5 nm
Neuromast fluid velocity detection threshold	T_V	$\frac{T_X}{S_V}$	1–10 (μm/s)
Lateral line organ fluid acceleration detection threshold	T_A	$\frac{T_V}{S_{can}}$	0.1–1 mm/s^2
Lateral line organ pressure difference detection threshold	$T_{\Delta p}$	$T_A \rho L$	0.1–1 mPa

Symbols are as used throughout the text and expressed in terms of measurable physical quantities. Numerical values relate to the ruffe, except for the hair cell displacement threshold, as indicated (*), which was taken from outer hair cells (van Netten et al. 2003).
f_t the transition frequency of a cupula (10 Hz; e.g. Eq. 11), N_r the cupular resonance number (64; e.g. Eq. 12), f_{can} the cut-off frequency of the lateral line canal, assuming a radius of 0.5 mm ($\sim$ 20 Hz;), kT the thermal noise energy ($4.1 \cdot 10^{-21}$ J), Z the molecular gating force of a hair cell transducer channel ($\sim$150 fN), N_{ch} the number of transducer channels per hair cell (80), K the cupular sliding stiffness (0.13 N/m), N the number of hair cells underlying a cupula (1,000), ρ fluid density (1,000 kg/m^3), L the effective distance over which a supra-orbital canal neuromast detects a pressure difference (1 mm)

used as a measure of the time constant of a resonating cupula (τ_r) as expressed in the right-hand side of (22).

Evaluation of (22) for the two types of resonating canal cupulae considered predicts envelope time constants of the cupular impulse response of about τ_r = 0.7 ms for the African knife fish and about τ_r = 3.8 ms for the ruffe. It thus seems inevitable that the ruffe, in the time domain, has to pay for its increased sensitivity ($S_r/S_r \cong 12$), obtained from enhanced cupular resonance, as compared to that of the African knife fish ($S_r/S_v \cong 7$). Recently, cupular responses to velocity impulses have been experimentally determined in the ruffe (Ćurčić-Blake and van Netten 2005). Time constants (τ_r) were found to be close (mean value, 4.4 ms) to the theoretical values considered here (3.8 ms). Detailed comparison of the impulse response measured and calculated with the linear cupular model (Eq. 10 or 13), however, also revealed differences that are most likely due to the nonlinear gating stiffness that reflects in the cupular sliding stiffness (e.g. van Netten and Khanna 1994; Sect. 2.11).

2.7 Threshold of velocity-sensitivity of lateral line cupulae

The sensory hair cells are the primary mechano-receptors of the lateral line organ and detect the displacement of the cupula. The displacement detection threshold of hair cells has recently been shown to be restricted by stochastic properties of the transducer channels and the Brownian gating spring noise (van Netten et al. 2003). The equivalent transducer related displacement noise ($T_{X,TD}$) was shown to be about $T_{X,TD} \cong 2kT/Z$, with kT ($\sim 4.1 \cdot 10^{-21}$ J) the thermal noise energy and Z ($\sim$ 150 fN) the molecular gating force of a hair cell's transducer channel, and was found to be about 6.5 nm per hair cell.

If the approximately 1,000 hair cells that underlie a ruffe supra-orbital canal cupula, all contribute independently but equally to the detection process (complete ensemble averaging), the effective displacement noise would decrease with a factor $\sqrt{1,000} \cong 32$, so that the overall equivalent hair cell displacement noise, may reduce to about 0.2 nm per neuromast. This number appears to be similar to the cupular Brownian motion that can be calculated for the ruffe's cupula with sliding stiffness K ($\sqrt{kT/K} \cong 0.2$ nm; e.g. Landau and Lifshitz 1983; $K \cong 0.13$ N/m, van Netten and Kroese 1987). The resulting overall (root summed squares) displacement detection threshold, $T_X \cong$0.3 nm, combined with the low frequency cupular velocity-sensitivity obtained for the ruffe ($S_v = 0.23\,\text{nm}/(\mu\text{m} \cdot \text{s}^{-1})$) thus leads to a threshold of cupular fluid velocity detection (T_V) of a neuromast of about $T_V = T_X/S_v \cong 1.3\,\mu$m/s under the assumed complete ensemble averaging conditions (cf. Table 1).

Alternatively, a threshold displacement value (T_X) of the supra-orbital canal cupula of ruffe has been obtained from extrapolating results of behavioral responses and was found to be one order of magnitude larger ($T_X \approx$2.5 nm; Kuiper 1956) than the value just estimated on the basis of transducer channel stochastics and Brownian motion ($\cong$ 0.3 nm). Correspondingly, this leads to a fluid velocity detection threshold (T_V) of the cupula of about 10 μm/s. This value is comparable to experimentally determined fluid velocity detection thresholds reported for the superficial lateral line organ (25 μm/s, Görner, 1963; 60 μm/s, Oman and Frishkopf, 1973; 38 μm/s, Kroese et al. 1978).

Combining the two approaches followed above leads to the conclusion that the ruffe's supra-orbital canal neuromasts may reliably detect fluid velocities in the canal with a threshold (T_V) ranging from about 1 to 10 μm/s.

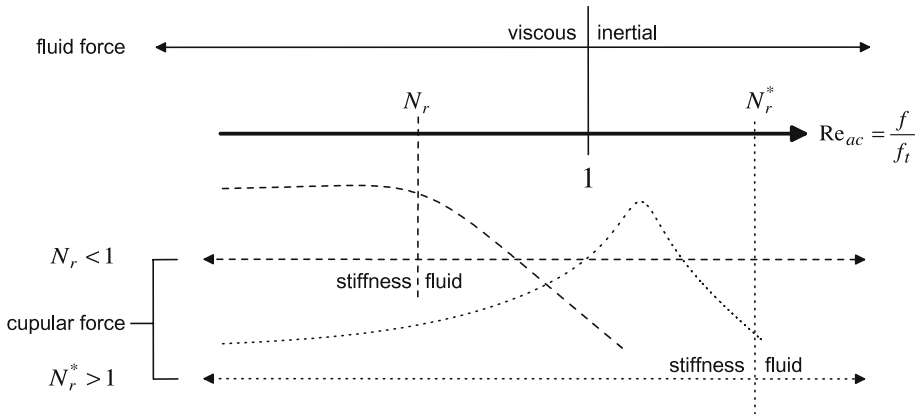

Fig. 5 Relation of resonance number, (N_r), to the a.c. Reynolds number ($Re_{\mathrm{a.c.}} = f/f_\mathrm{t}$), which denotes the position of frequency on the normalized frequency-axis (11). Two different N_r numbers are distinguished, corresponding to a velocity detector ($N_\mathrm{r} < 1$; *dashed lines*) and a resonating cupula ($N_\mathrm{r}^* > 1$; *dotted lines*). The value 1 on the normalized frequency-axis separates the viscous- from the inertial dominated frequency regions. The positions of the N_r numbers on this axis mark the frequencies at which fluid forces take over dominance over the stiffness forces acting on a cupula

2.8 Physical significance of the resonance number, N_r

The dimensionless resonance number, N_r (12), has been shown to play a pivotal role in cupular dynamics. Dimensionless numbers are quite common in the description of physical phenomena and are specifically used in hydrodynamics to determine how the physical parameters of a system can be simultaneously modified while keeping the same response. In the same fluid, different cupular configurations possessing an equal product of cupular sliding stiffness times cupular radius (Ka = constant) have the same value for N_r (12). Such cupulae thus share the same frequency characteristics, apart from the scaling of the frequency axis with f_t (11).

Many dimensionless numbers in fluid dynamics are defined as the ratio of two types of forces. The best-known example is the Reynolds number, $Re_\mathrm{dc} = \rho a V_\mathrm{dc}/\mu$ for steady (d.c.) flow with velocity (V_dc) past an object with characteristic dimension a, which can be compared to the (a.c.) Reynolds number, $Re_\mathrm{ac} = f/f_\mathrm{t} = 2\pi a^2 f/\mu$ for periodic flow (cf. Eq. 11). Both types of Reynolds numbers represent the ratio of viscous to inertial fluid forces.

The resonance number, N_r (12) appears to define the absolute ratio of the stiffness force acting on an object, elastically suspended via stiffness K, and the Stokes fluid force acting on it, when vibrating at the transition frequency f_t (11), at which viscous and inertial forces balance, in a fluid at rest (at infinity):

$$\left| \frac{KY}{6\pi a \mu \dot{Y}_{f=f_\mathrm{t}}} \right| = \frac{K}{6\pi a \mu (2\pi f_\mathrm{t})} = N_\mathrm{r}. \tag{23}$$

The significance of the resonance number is further summarized in Fig. 5 in relation to the a.c. Reynolds number ($Re_\mathrm{ac} = f/f_\mathrm{t}$), which effectively represents the normalized frequency axis (cf. Eq. 11). The value 1 on this frequency axis (Fig. 5) separates viscous- from inertial dominated frequency regions in terms of vibratory fluid forces acting on the cupula. N_r marks the normalized cut-off frequency, f_c (15), which represents the upper bound of frequencies of excitatory fluid velocity that result in a significant vibration amplitude of the object (i.e. $S(f) \geqslant S_v$).

Similar to the discriminative role of the Reynolds number, the resonance number, (N_r) separates the frequency regions of dominance of stiffness – ($Re_\mathrm{ac} < N_\mathrm{r}$) versus fluid forces ($Re_\mathrm{ac} > N_\mathrm{r}$) acting on the cupula. In case of the latter condition, the fluid force at N_r is either of a viscous – ($N_\mathrm{r} < 1$) or of an inertial nature ($N_\mathrm{r} > 1$), as can be seen from Fig. 5.

Since the cupular sliding stiffness derives from the collective stiffness of the hair bundles of the hair cells underlying the cupula, information on the bundles' micromechanical properties may be obtained in studies on cupular mechanics employing frequencies in the stiffness dominated region (e.g. van Netten and Khanna 1994; van Netten et al. 1994; Wiersinga-Post and van Netten 1998).

The basic arrangement of the cupular excitation model considered consists of an elastically suspended mass with stiffness coupling K, and characteristic dimension a, both driven and damped by a fluid characterized by its density (ρ) and viscosity (μ). Such an arrangement is not unique to cupulae of the lateral line system and the classification by means of the resonance number can thus be expected to outreach this context. Its usefulness can accordingly be expected in the fields of vestibular- and hearing research, for instance in investigating the hydrodynamic excitation of free-standing hair cell bundles (e.g. van Netten 1997; Géléoc et al. 1997) as well as in other practical applications of mechano-receptive devices.

2.9 Prediction of N_r for superficial neuromasts

Since the resonance number (N_r) in canal neuromasts, at least in the cases investigated, yields values larger than one, the question arises whether superficial cupulae may possess (N_r) values smaller than 1 so that they exhibit pure low-pass velocity detecting characteristics, as suggested by electrophysio-

logical data of their afferent activity (Görner 1963; Strelioff and Honrubia 1978; Kroese et al. 1978; Kroese and Schellart 1992; Engelmann et al. 2000, 2002).

Superficial neuromasts have their cupula protruding into the water surrounding the animal. In water ($\rho = 1,000$ kg/m^3; $\mu = 0.001$ Pa · s), the condition $N_r < 1$ reduces to an upper bound on the product of the stiffness and cupular radius ($Ka < 19$ nN).

The sliding stiffness (K) of canal neuromasts can almost exclusively be attributed to the collective stiffness of its about a thousand hair bundles (van Netten and Kroese 1987, 1989; van Maarseveen 1994). A smaller stiffness is therefore likely to result from the tens of hair bundles that usually underlie superficial cupulae, which may vary in stiffness from 0.1 to 1 mN/m per hair cell bundle, depending on hair bundle length. Furthermore, the cupulae of superficial neuromasts are smaller than the canal cupulae investigated. Together, these two factors predict values of the order of 10–100 nN for the stiffness-radius product (Ka) of superficial neuromasts. This suggests that superficial neuromasts can probably be classified as detectors of fluid velocity in a considerable frequency range and do not likely exhibit strong resonance.

Complicating factors may arise from the more elongated shapes that superficial cupulae possess and their presumably more flexible structure as compared to that of canal cupulae, which move as rigid structures (van Netten and Kroese 1987; Kelly and van Netten 1991). Also, because of the limited extent to which superficial cupulae penetrate into the surrounding water, the boundary layer along the skin is likely to affect more strongly the velocity sensed by a superficial cupula as compared to a canal cupula (e.g. Jielof et al. 1952; Kalmijn 1988).

Mechanical measurements on superficial neuromast dynamics are still pending but are required to investigate whether the cupular model of excitation used for canal neuromasts is also applicable to superficial neuromasts.

2.10 Matched cupular- and hair cell filtering

The mechanical frequency responses of the canal neuromasts investigated have been shown to match the frequency characteristics of extracellular receptor potentials of the mechano-transducing hair cells under the temperature conditions of their habitat, which is about 4°C for the ruffe and above 25°C for the tropical African knife fish (Wiersinga-Post and van Netten 2000). Adaptation of these different fish species to their natural habitat and relevant stimuli may have shaped these two subsequent stages of peripheral filtering so as to optimize the signal-to-noise-ratio.

Applying the results of cupular mechanics to different species, we may predict a variety in dynamics given the morphological diversity in the lateral line system that has been described (Coombs et al. 1988, 1992; Webb 1989; Münz 1989). It has nevertheless been reported that the afferent activity of morphologically different canal neuromasts in Antarctic fish points to converging frequency characteristics (Coombs and Montgomery 1992; Montgomery et al. 1994). A factor that may be related to this observation is that cupular dimension and the number of hair cells that fit the cupular base area are most likely related, so that cupular radius (a) and the stiffness of the elastic hair bundle coupling to the canal (K) are correlated. Such a correlation causes the detection bandwidth of cupulae within a considerable range of different dimensions and related stiffnesses to be confined to a relatively restricted frequency range (e.g. van Netten 1991).

2.11 Hair cell transduction in the lateral line organ

The lateral line organ has been, and still is, frequently used as a model to study fundamental aspects of hair cell transduction (e.g. Jielof et al. 1952; Kuiper 1956; Flock 1965; Harris et al. 1970; Russell 1976; Sand 1984; van Netten and Khanna 1994; Wiersinga-Post and van Netten 1998; Nicolson et al. 1998; Sidi et al. 2003; Söllner et al. 2004; Corey et al. 2004). Also specific blockers of the hair cell transducer channels have been investigated using electrophysiological recordings of the lateral line organ (Kroese and van den Bercken 1980, 1982; Karlsen and sand 1987; van Netten et al. 1994; Wiersinga-Post and van Netten 1998).

Biophysical studies of the transducer channels in bullfrog saccular hair cells have provided many fundamental properties of the molecular mechanisms responsible for the opening of the channel's gates in response to hair bundle motion (e.g. Howard and Hudspeth 1988; Markin and Hudspeth 1995). These properties include the force required to open a single transducer channel, the swing of the channel upon opening and the stiffness of the elastic gating springs that engage each channel's gate. The gating spring in combination with the mechanical coupling to the channel's gate on one side and the hair bundle on the other side gives rise to a reduction in hair bundle stiffness (gating compliance) which depends on the deflection of the hair bundle. Similar nonlinearities in bundle stiffness were reported in mammalian and other hair cell types studied in vitro (Russell et al. 1992; Géléoc et al. 1997; van Netten and Kros 2000; Ricci et al. 2002). Studies on the motion of the cupula in response to fluid flow past it has revealed nonlinear behavior that could be explained by the nonlinear gating compliance of the transducer channels (van Netten and Khanna 1994). Analysis of these mechanical nonlinearities of the lateral line cupula thus enabled the determination of molecular properties like gating force under in vivo conditions in an intact hair cell organ, and were found to resemble those found in in vitro studies.

Hair cell bundles of the bullfrog's sacculus have also been reported to display complex active behavior, as reflected in spontaneous motion, which was explained by an interplay between a negative stiffness associated with the gating compliance and molecular motors that are involved in calcium-dependent hair cell adaptation (Hudspeth et al. 2000). Signs of spontaneous active mechanical behavior so far have not been reported for cupular dynamics, but are also likely to be suppressed by the mutual mechanical coupling of tens

to thousands of hair cell bundles via their overlying cupula. Detailed investigation of possible power-law behavior of the input–output relationship of cupular responses at threshold (< 1 nm) may give indications as to whether similar mechanisms as found in individual bundles of the bullfrog's sacculus (Martin et al. 2003) enhance the detection properties of the lateral line organ (see also Sect. 3.4).

3 Canal hydrodynamics and lateral line sensitivity

3.1 Velocity flow profiles in canals

Motion of water surrounding the fish is first transferred into canal fluid motion before a canal cupula is excited. Denton and Gray (1983) experimentally investigated the filter characteristics of the transmission step of outside water motion into canal fluid motion. Their theoretical approach to explain their observations was based on a lumped parameter model, representing fluid inertia and viscous resistance (Denton and Gray 1983, 1988, 1989).

Here a solution of the Navier–Stokes equation will be considered, which describes the velocity of a viscous fluid inside a canal, as resulting from an oscillatory pressure with a constant amplitude gradient along the canal. The solution is originally due to Sexl (1930), and has been applied by Womersley (1955) to describe pulsating blood flow in arteries, while specific numerical solutions are discussed by Schlichting (1979).

Canal neuromasts are now commonly described as detectors of outside water acceleration (e.g. Denton and Gray 1983; Kalmijn 1988; Coombs and Janssen 1990; Kroese and Schellart 1992; Wubbels 1992; Engelmann et al. 2002). It is therefore useful to express the fluid velocity inside the canal in response to acceleration of water outside the canal. Assuming potential flow outside the fish causing the water motion relative to the fish, a pressure gradient corresponds to water acceleration (A) via $dp/dx = -\rho A$, where ρ is the density of water (e.g. Denton and Gray 1982; Kalmijn 1988). Sexl's (1930) original solution for the velocity inside a canal can then be expressed in terms of periodic outside water acceleration, $A(t) = A_0 \exp(i2\pi f t)$. Then, the complex steady-state velocity amplitude ($V_0(r, f)$) of the oscillatory laminar fluid flow inside a circular canal with radius (R) at distance (r) from the canal axis, divided by the excitatory acceleration amplitude of water outside the canal (A_0) can be defined as the canal sensitivity [$S_{\text{can}}(r, f)$] and is given by (e.g. Sexl 1930; Womersley 1955; Schlichting 1970):

$$S_{\text{can}}(r, f) = \frac{V_0(r, f)}{A_0} = \frac{-i}{2\pi f}\left[1 - \frac{J_0\left(\sqrt{-2i}\,\frac{r}{\delta}\right)}{J_0\left(\sqrt{-2i}\,\frac{R}{\delta}\right)}\right]. \quad (24)$$

An appropriate unit for the canal sensitivity is (μm/s) / (mm/s^2) which is equivalent to millisecond, and is thus similar to the unit that can be used to express cupular sensitivity (e.g. Sect. 2.4 and Eq. 21). To calculate numerically the fluid flow profiles in the canal, the Bessel functions of the first kind and order zero (J_0) with a complex argument having a phase of $-\frac{1}{4}\pi$ (24) were evaluated in terms of the Bessel–Kelvin functions ($J_0(\sqrt{-i} \cdot x) = ber_0(x) + i \cdot bei_0(x)$; e.g. Mathews and Walker 1970). The calculated flow profiles are frequency dependent, also via the boundary layer with thickness (δ) defined similarly to that of a sphere ($\delta = \sqrt{\mu/(\rho\pi f)}$; cf. Eq. 4).

Figure 6 gives examples at three frequencies (2, 20 and 200 Hz) of the circle-symmetrical laminar fluid flow profiles across the cross-section of a circular canal, calculated at eight different points in time normalized to their respective periods (Fig. 6d). The canal diameter was assumed to equal that of the supra-orbital canal in ruffe (Ø = 1 mm; e.g. Fig. 1a).

At low frequencies ($\sim$ 2 Hz; Fig. 6a), viscous forces dominate and cause flow velocity with parabolic profiles, which are in phase with the water acceleration outside the canal, $A(t)$ (Fig. 6d).

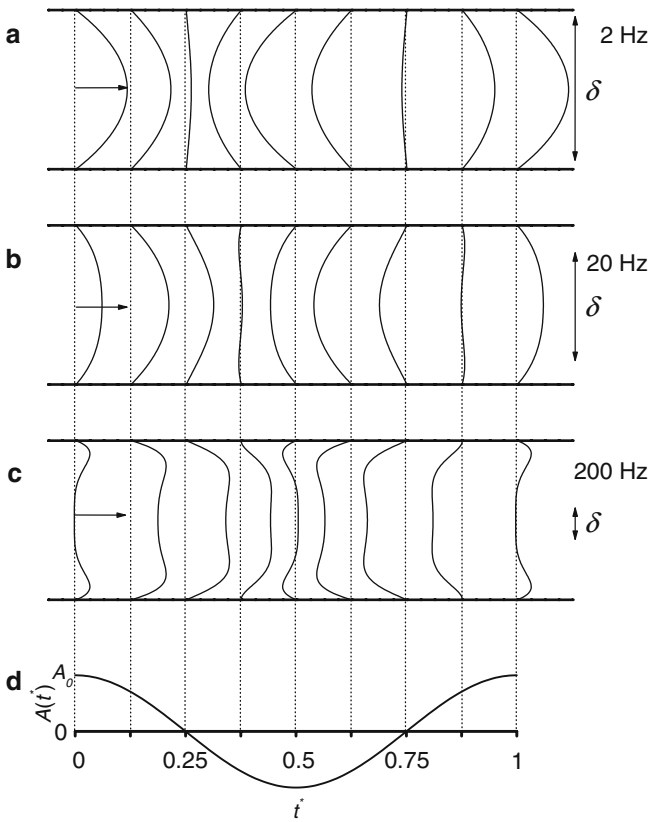

Fig. 6 Fluid flow profiles across a canal with radius, $R = 0.5$ mm, calculated with (24) at the three frequencies indicated (**a**: 2 Hz; **b**: 20 Hz; **c**: 200 Hz; after Schlichting 1979). Viscosity was 0.005 kg/ms (e.g. van Netten and Kroese 1987). The profiles depicted between *thick lines* representing the canal walls, are related via *dotted vertical lines* to the different phases, indicated with the period-normalized time, t^* (**d**) of the acceleration of water outside the canal, $A(t^*)$. Horizontal (single) arrows indicate the canal sensitivity, $S_{\text{can}}(r, f)$ (24) measured as fluid velocity inside per water acceleration outside and are expressed as (μm/s)/(mm/s^2) which equals millisecond. The length of the arrows is 100 ms in **a** and **b** and 10 ms in **c**. The *three vertical (double) arrows* indicate the boundary layer thickness, (δ) in the canal referenced to the diameter of the canal

At intermediate frequencies (~ 20 Hz; Fig. 6b) profiles are produced by both viscous and inertial forces and result in parabolic-like profiles with a phase that lags the outside acceleration with about 45°.

At high frequencies (~ 200 Hz; Fig. 6c) inertial fluid forces cause annular profiles with a central region within which the fluid velocity is fairly constant. In the high frequency limit, the maximum amplitude is thus not reached at the axis of the canal but instead at a distance of about 2.3 times the boundary layer thickness from the wall ($2.28 \cdot \delta$; Schlichting 1979). A similar shift towards the canal wall of the velocity maximum has been observed by directly measuring fluid velocity profiles in fenestrated supra-orbital lateral line canals of the ruffe (Tsang and van Netten 1997). At high frequencies, the phase of inside fluid velocity lags behind that of the outside acceleration (Fig. 6d) by about 90°. Across the canal diameter, however, relatively small phase differences occur.

The calculated frequency dependence of the canal sensitivity at the axis of the canal [$S_{can}(0, f)$] is depicted in more detail in Fig. 7 (dash-dot lines; canal Ø = 1 mm). In terms of fluid velocity inside, the supra-orbital lateral line canal in ruffe thus acts approximately as a first-order low-pass filter of outside water acceleration with a cut-off frequency (f_{can}) of approximately 20 Hz, beyond which the amplitude rolls of with 20 dB/decade (Fig. 7). These results are in good agreement with experiments performed in real and artificial lateral line canals in which fluid velocity has been measured (Denton and Gray 1983, 1988).

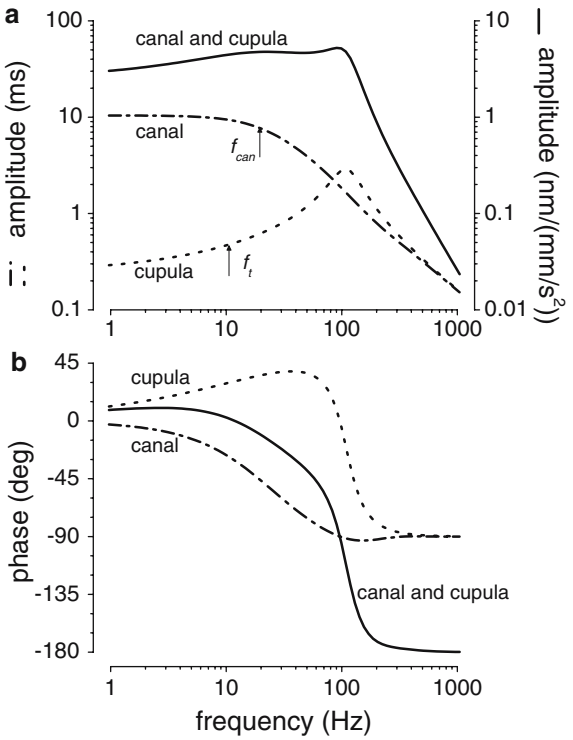

Fig. 7 Sensitivity of overall peripheral canal lateral line filtering in ruffe. **a** Amplitude of canal sensitivity ($S_{can}(0, f)$; *dash-dotted*) and cupular sensitivity ($S(f)$; *dotted line*), which can both be expressed in ms (left ordinate). The amplitude of the combined sensitivity of canal and cupula ($S_{llo}(f)$; *solid line*) is expressed in nm/(mm/s^2) which equals ms^2 (*right ordinate*). **b** Phase of sensitivities (same line codes as in **a**). The phase of canal sensitivity is referred to outside water acceleration, whereas the phase of cupular sensitivity is referred to (canal) fluid velocity. Therefore, the phase of the combined sensitivity is referred to the outside water acceleration. Arrows in (**a**) show that the cupular transition frequency, f_t, (~ 10 Hz) and canal cut-off frequency, f_{can} (~ 20 Hz) are comparable

3.2 Combined canal- and cupular filtering

To illustrate the combined hydrodynamic filter action of the canal and the cupula, the fitted cupular sensitivity of the ruffe, as shown in Fig. 4, has been replotted in Fig. 7 (dashed lines). Multiplying the sensitivity curves of the cupula with that determined for the canal (dash-dot lines, Fig. 7) results in the overall peripheral sensitivity of the canal lateral line organ, $S_{llo}(f) = S_{can}(0, f) \cdot S(f)$ (Fig. 7, solid lines). Both canal and cupular sensitivity can be expressed as millisecond (left ordinate), whereas the overall sensitivity amplitude is expressed as cupular displacement in nanometer, per outside water acceleration in mm/s^2, i.e. nm/(mm/s^2) which equals ms^2 (Fig. 7a, right ordinate).

From f_{can} to about the cupular resonance frequency (~ 120 Hz) cupular sensitivity [$S(f)$] increases with frequency with about the same rate at which the canal sensitivity [$S_{can}(f)$] decreases. The overall sensitivity [$S_{llo}(f)$] therefore results in an almost constant value (~ 4 nm/(mm/s^2) or ~ 4 ms^2) from low frequencies (~ 1 Hz) to a frequency somewhat below the cupular resonance frequency (~ 100 Hz), with hardly any sign of cupular resonance. Since both canal- and cupular sensitivity fall with 20 dB/decade in the frequency range beyond cupular resonance, the combined sensitivity [$S_{llo}(f)$] rolls of at approximately 40 dB/decade at these frequencies.

The cupula in the supra-orbital canal of the ruffe can thus be considered to be a detector of outside water acceleration up to frequencies of about 100 Hz. This conclusion is in line with measured extracellular receptor potentials in the ruffe's canal lateral line (Kroese and van Netten (1989)) and with afferent recordings of canal neuromasts of the ruffe (Wubbels 1992) and of other fish species (Münz 1985; Kroese and Schellart 1992; Coombs and Janssen 1990; Coombs and Montgomery 1992).

Also, previous work on hydrodynamic field detection implied acceleration sensitivity of canal neuromasts (Denton and Gray 1983; Kalmijn 1988). The precise characteristics of the underlying mechanisms for the acceleration detection of the canal lateral line that is observed here are nonetheless somewhat different from the mechanisms proposed for it before. Previously, the actions of two cascaded filters, a first-order low-pass filter effected by the canal and an additional velocity sensitive cupular filter, also acting as a first-order low-pass filter, were implied to explain acceleration detection. Here, it is shown that the enhanced cupular sensitivity

resulting from resonance makes up for the decreased canal sensitivity beyond about 20 Hz, resulting in a flat acceleration sensitivity up to about 100 Hz.

Such compensatory effects of canal - and cupular filtering may occur more generally, since the frequency at which the canal starts to attenuate the flow (f_{can}) is in general similar to the transition frequency (f_{t}) at which a resonating cupula starts to have increased sensitivity. This similarity of both frequencies can be seen from comparing the cut-off frequency of a canal (f_{can}) having radius R $f_{\mathrm{can}} \cong 5\mu/(2\pi\rho R^2)$(cf. Schlichting 1979), which is about 20 Hz for the ruffe, with the transition frequency defined by $f_{\mathrm{t}} = \mu/(2\pi\rho\, a^2)$ (11), which is about 10 Hz for the ruffe. A cupula with a radius, a, which is a considerable fraction,ε, of the canal radius, R, (i.e.$a = \varepsilon R; 0 < \varepsilon < 1$), thus has comparable values for both frequencies ($f_{\mathrm{t}} \cong f_{\mathrm{can}}/\left(5\varepsilon^2\right)$). Therefore, the combination of these two peripheral lateral line filters in general tends to produce a constant acceleration sensitivity up to almost the resonance frequency of a cupula.

Additional significant filtering or possible resonance arising from the compliance of the skin overlying the canal, as observed in the wide (Ø ≅ 7 mm) cephalic canals of *Poromitra* (Denton and Gray 1988), has not been observed in the supra-orbital canal of the ruffe (van Netten and van Maarseveen 1994).

Functionally, the constant acceleration detection characteristics of the canal lateral line organ may be of significant importance, as it renders the lateral line canal organ insensitive to stationary fluid flow (Coombs and Montgomery 1992; Montgomery et al. 1994).

3.3 Acceleration and pressure gradient detection threshold of the canal lateral line organ

The sensitivity of a lateral line canal, S_{can}, in the center and at frequencies below f_{can}, in the ruffe amounts to about $S_{\mathrm{can}}(0,0) \cong 1/(2\pi f_{\mathrm{can}}) \cong \rho R^2/(5\mu) \cong 10\,(\mu\mathrm{m/s})/(\mathrm{mm/s^2})$ or equivalently, 10 ms (Fig. 7). Note that a similar sensitivity-bandwidth principle as was described for cupular hydrodynamics (20) is therefore imposed on canal hydrodynamics. Combining the canal sensitivity ($S_{\mathrm{can}} \approx 10$ ms; Fig. 7) with the estimate of the threshold value of cupular velocity detection ($(T_V) \approx 1$–$10\,\mu$ m/s; see Sect. 2.7), yields a fluid acceleration detection threshold, (T_A), of the canal lateral line organ of about $T_A = T_V/S_{\mathrm{can}} \approx 0.1$ to 1 mm/s^2 (cf. Table 1). A similar value for the threshold of water acceleration detection was observed for the head canal lateral line organ of mottled sculpin (*Cottus bairdi*, Coombs and Janssen 1990).

The relationship between fluid acceleration, (A), and the pressure gradient in a free volume of water ($dp/dx = -\rho A$, see Sect. 3.1) also allows for an interpretation of the acceleration threshold just estimated, in terms of a pressure difference detection threshold. Since the typical dimensions of the length, (L), of the canal over which a ruffe supra-orbital cupula detects a pressure gradient is of the order of 1 mm (e.g. van Maarseveen 1994), we arrive at an estimate of an effective pressure difference threshold of $T_{\Delta p} = \rho T_A L \approx 0.1$ to 1 mPa for the canal lateral line organ (cf. Table 1). Pressure differences of the same order of magnitude have been measured across the ruffe's lateral line canal while the cupula was moving in the displacement threshold range of nanometers (van Maarseveen 1994).

3.4 Comparison of near field detection threshold in the lateral line organ and the mammalian inner ear

Given the morphological differences between the lateral line system and the mammalian hearing organ, which can be classified as a pressure-detecting sense organ based on hair cells (e.g. von Békésy 1960), it may not be obvious that both organs would possess comparable pressure detection threshold levels. Yet, comparing the threshold of hydrodynamic pressure difference detection of the lateral line organ (0.1 – 1 mPa; Sect. 3.3), with an estimate of pressure detection in the inner ear (0.6 mPa), shows that both values are comparable. This order of magnitude estimate of near field pressure detection level in the inner ear is based on the threshold value of sound detection (0 dB, SPL $\approx 20\,\mu$Pa in air) in combination with assuming a pressure gain of about 30 dB in the transfer of air pressure to inner ear fluid pressure by the middle ear (e.g. de Boer 1980; Olson 1998).

Since the pressure threshold values of both sensory organs are based on the assumption of a similar intrinsic level of hair cell accuracy (van Netten et al. 2003), their equivalent detection threshold level may essentially point to comparable efficiencies of hydrodynamic pressure transfer to the mechano-detecting hair bundles of the hair cells. An important difference that is related to the differences in architecture between both mechano-sensory organs is the high-frequency limit, which in some mammalian hearing organs may be up to three orders of magnitude higher than that of the lateral line organ.

A Appendix

A.1 Near- and far field of a hydrodynamic dipole stimulus

In many physiological experiments on the lateral line system, a submerged moving sphere suitably located in close proximity to a neuromast or placed in a lateral line canal, has been used to produce hydrodynamic near fields to effectively stimulate lateral line cupulae. This type of stimulus is usually referred to as a dipole source. In most experimental protocols the sphere exerts sinusoidal displacements at various frequencies, facilitating the straightforward measurement of frequency responses of a neuromast.

When dipole sources for lateral line stimulation are considered, a clear distinction has to be made between the local and far field produced by the vibrating sphere, which are characterized with respect to the distance to the sphere's center,

r. The far field is the dominant flow component in regions more distant from the sphere. The pressure of this component falls with distance as $r^{-1}$and is usually referred to as the sound produced by the stimulus sphere. The local or near field pressure, sometimes called the hydrodynamic component as opposed to the sound (far field) component, falls with $r^{-2}$and can be shown to be most relevant to lateral line stimulation as it is the predominating component close to the source (Harris and van Bergeijk 1962; Kalmijn 1988, 1989; Coombs and Montgomery 1999). This can be appreciated from considering that the near- and far field components of the total flow field of a dipole change their dominance in amplitude approximately at a distance, (r_t), from the sphere of the order of the wavelength $r_t \approx \lambda/(2\pi) = c/(2\pi f)$ (e.g. Kalmijn 1988). Here the wavelength, (λ) is alternatively expressed via the frequency of stimulation, (f) and the velocity of sound propagation c (~1440 m/s in water). Since the lateral line organ is mainly operational in the frequency range from d.c. up to the order of hundred Hertz, evaluation of r_t yields that the near field extends into a region of at least meters around the source. This clearly covers the distances over which the lateral line obtains its main input (Dijkgraaf 1963).

An extensive overview of the acoustic and hydrodynamic field of a dipole source in relation to the lateral line organ has been given previously (Kalmijn 1988). However, as in most quantitative experimental investigations of the lateral line organ (e.g. Kroese et al. 1978; Kroese and Schellart 1992; Kalmijn 1988, 1989; Coombs et al. 1996; Coombs and Montgomery 1999), the effects of fluid viscosity were omitted so that only the irrotational (potential) flow is considered, although the significance of a viscous boundary layer in this respect has been recognized (Kalmijn 1988).

In the next section, we will consider the near field produced by a vibrating sphere while viscosity will be included. Incorporating viscosity, gives a more complete picture of the near field flow since it also includes the boundary layer around the sphere. Comparison with solutions of inviscid potential flow shows that the viscously induced frequency dependent boundary layer around the sphere, in which rotational flow effectively changes to potential flow (e.g. Landau and Lifshitz 1987) introduces both phase and amplitude differences that may significantly affect the produced stimuli by small spheres at relatively low frequencies, even outside the boundary layer.

A.2 Viscous boundary layer affects amplitude and phase of vibratory dipole lateral line stimuli

Stokes' analysis (1851) and later treatments (e.g. Lamb 1931) of the hydrodynamic near field created by a vibrating sphere comprise one of the few examples of vibrating solid structures in a viscous fluid for which analytical expressions were derived for the fluid pressure and velocity fields.

As in Sect. 2.2, we consider here Stokes' solution of the near field in a viscous fluid produced under free field conditions by a rigid sphere with radius a vibrating with frequency $f = \omega/(2\pi)$, and amplitude B, so that the sphere's displacement is given by $X = B \sin \omega t$. The result for the pressure is equivalent to (3), but now rewritten in terms of a dimensionless correction factor C and phase delayφ, both with respect to the (inviscid) potential flow ($C = 1$; $\varphi = 0$) case:

$$p(r,\theta) = -C \cdot \frac{\rho\, a^3 \omega^2 \cos\theta}{2r^2} B \sin(\omega t - \varphi). \tag{25}$$

C and φ depend on the ratio of boundary layer thickness, (δ), and sphere radius (a), via the functions C_1 and C_2:

$$C = \sqrt{C_1^2 + C_2^2};\ \varphi = \arctan\left(C_2/C_1\right), \tag{26}$$

which were already defined in Eqs. 4–6:

$$C_1 = 1 + \left(\frac{3\delta}{2a}\right), C_2 = \left(\frac{3\delta}{2a}\right)\left[1 + \left(\frac{\delta}{a}\right)\right]$$

$$\text{and } \delta(\omega) = \sqrt{\frac{2\mu}{\rho\omega}}. \tag{27}$$

The effects of the viscous boundary layer on the pressure field thus become less significant if its thickness is considerably smaller than the sphere's diameter ($\delta << a$). This occurs in the high frequency regime [i.e. if $\omega >> 2\mu/(\rho\pi a^2)$], so that $C \to 1$, while $\varphi \to 0$ (Eqs. 26 and 27), which means that the high frequency regime of the pressure distribution is equivalent to neglecting viscosity ($\mu = 0$, leading directly to $\delta = 0$). Equations 25–27 show that the viscosity results in a frequency dependent increase in pressure amplitude with a correction factor, $C(> 1)$, and causes a phase delay,(φ) as compared to inviscid potential flow.

Both quantities are shown in Fig. 8 as a function of stimulus frequency, $f = \omega/(2\pi)$, for three different diameters of a sphere vibrating in canal fluid (e.g. van Netten 1991). The effect of viscosity on the pressure appears to be significant when stimulating the lateral line with a sphere having millimeter dimensions at frequencies of the order of a few Hertz and below.

The radial,(v_r), and tangential, (v_θ), velocity distribution around the sphere can be calculated by taking derivatives of the related stream function as described in Stokes' work (1851). The result is:

$$\begin{aligned} v_r = &-\mathrm{e}^{-\beta} \cdot \frac{3a\delta\, \cos\theta}{2r^2} B\omega \\ &\times \left[\cos(\omega t - \beta) + \left(1 + \frac{\delta}{r}\right)\sin(\omega t - \beta)\right] \\ &+ \frac{a^3 \cos\theta}{r^3} C B\omega \cos(\omega t - \varphi), \end{aligned} \tag{28}$$

$$\begin{aligned} v_\theta = \mathrm{e}^{-\beta} \cdot \frac{a \sin\theta}{2r} B\omega \Bigg[&-3\left(1 + \frac{\delta}{2r}\right)\cos(\omega t - \beta) \\ &-\frac{3}{2}\frac{\delta}{r}\left(1 + \frac{\delta}{r}\right)\sin(\omega t - \beta)\Bigg] \\ &+ \frac{a^3 \sin\theta}{2r^3} C B\omega \cos(\omega t - \varphi), \end{aligned} \tag{29}$$

with

$$\beta = \frac{r - a}{\delta}. \tag{30}$$

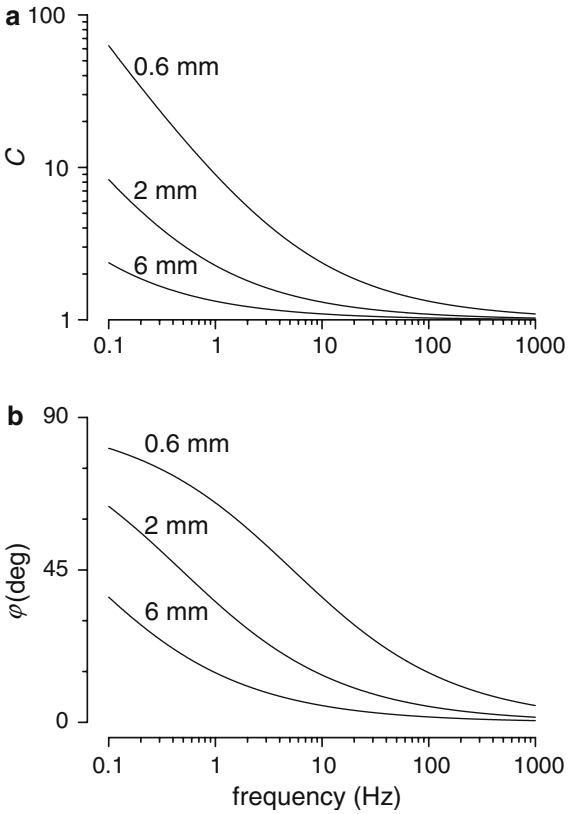

Fig. 8 Effect of viscosity (5 mPa·s) on pressure amplitude and phase as compared to potential flow. **a** The amplitude is increased with a factor $C = \sqrt{C_1^2 + C_2^2}$, **b** the pressure's phase is delayed by $\varphi = \arctan(C_2/C_1)$ (Eqs. 25, 27), as is shown for a range of frequencies relevant to the lateral line organ and for sphere diameters, of 0.6, 2 and 6 mm, as indicated

Both radial and tangential velocities (Eqs. 28 and 29) contain two terms, of which the first in each case gives only a significant contribution in the boundary layer ($a \leqslant r <$

►

$a + \delta(\omega)$) because of their proportionality with the factor $\exp(-\beta)$, which vanishes quickly with distance, r, outside this layer. These terms thus describe the transitions in fluid velocity between the sphere's boundary, on which the no slip condition holds, and the field outside the boundary layer.

Because radial and tangential velocities are not in phase (Eqs. 28 and 29), the flow is clearly rotational in, but also extending in a region outside of the boundary layer especially around angles at 45°, 135°, 225° and 315° with the vibra-

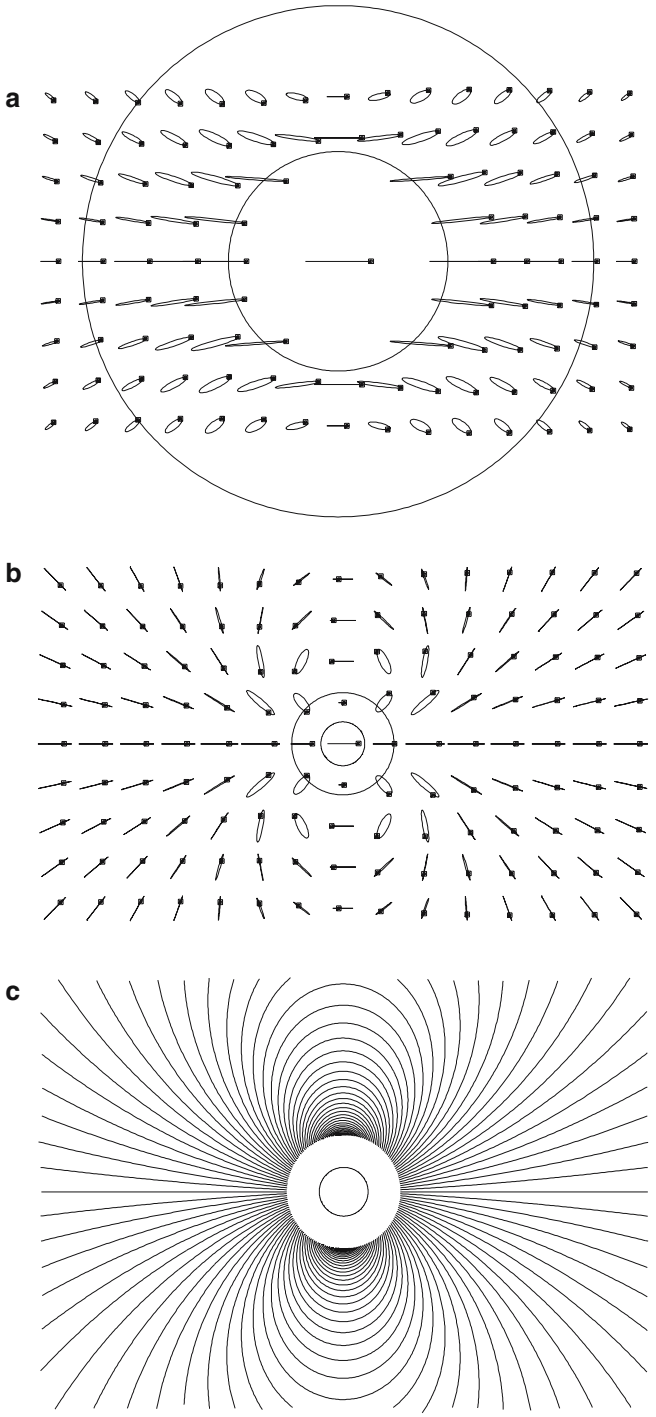

Fig. 9 Velocity flow produced by a sphere with a diameter of 0.6 mm and vibrating at 10 Hz in canal fluid with a viscosity of 5 mPa·s, as calculated by Eqs. 28–30. **a** The *inner circle* represents the sphere's boundary, while the *outer circle* indicates the extent of the boundary layer as calculated with Eq. 4. The flow trajectories shown indicate the pathways that a fluid particle's velocity vector points to during one cycle. The velocity vectors' origins lie in the center of each trajectory and represent the location of the associated flow. The mutual phase relationship of the velocity trajectories and their relation to that of the sphere's velocity is marked by a *square*. The velocity amplitude of the *sphere*, to which the amplitudes of the trajectories are scaled, is indicated by the line in the *inner circle* and its phase mark (*square*) corresponds to the phase of maximum rightward velocity. **b** Same flow field as depicted in *a*, but in an extended region around the *sphere*. To compensate for the rapid fall-of of the velocity amplitudes with distance, r, outside the boundary layer the trajectory dimensions are multiplied by r^3. The constant phase delay ($\varphi \approx 36°$) of the flow outside the boundary layer is clearly visible. Also, the phase reversal with increasing distance at $\theta = 90$ and 270° is evident. **c** Streamlines of inviscid potential dipole flow. The resemblance with the viscous flow trajectories outside the boundary layer, as depicted in **b** is obvious

tional axis, as can be seen from the elliptical pathways that the fluid velocity follows during one cycle (Figs. 9a and 9b). The second terms in both expressions represent the velocity components that remain (far) outside the boundary layer as previously described (van Netten 1991). These terms decrease with the cube of the distance, r^{-3}, and, similar to the pressure distribution (Eqs. 25–27), are increased by a factor C relative to potential flow and delayed in phase with $\varphi = \arctan(C_2/C_1)$ as compared with the sphere's velocity ($B\omega\cos(\omega t)$). As the two velocity components, v_r and v_θ are equally delayed in phase outside the boundary layer, the elliptical pathways are reduced to overlying trajectories of the back and forth phases of one cycle, which, when connected, form the streamlines of the potential flow of a dipole (Fig. 9c) as can be seen from comparison with Fig. 9b.

Acknowledgements The author thanks A.B.A. Kroese, D.G. Stavenga and C.J. Kros for their comments on a previous version of the manuscript.

References

Abdel-Latif H, Hassan ES, von Campenhausen C (1990) Sensory performance of blind Mexican cave fish after destruction of the canal neuromasts. Naturwissenschaften 77:237–239

Batchelor GK (1967) An introduction to fluid mechanics. Cambridge University Press, Cambridge

von Békésy G (1960) Experiments in hearing. ASA AIP report, McGraw-Hill, New York

Bleckmann H (1980) Reaction time and stimulus frequency in prey localization in the surface-feeding fish *Aplocheilus lineatus*. J Comp Physiol A 140:163–172

Bleckmann H (1993) Role of the lateral line in fish behaviour. In: Pitcher TJ (ed) Behaviour of Teleost fishes. 2nd edn. Chapman & Hall, London pp 201–246

Bleckmann H, Breithaupt T Blickhan R, Tautz J (1991) The time course and frequency content of hydrodynamic events caused by moving fish, frogs and crustaceans. J Comp Physiol A 168:749–757

de Boer E (1980) Auditory physics. Physical principles in hearing theory. I Phys reports 62:87–174

Cahn PH (1967) Lateral line detectors. Indiana University Press, Bloomington

Ćurčić-Blake B, van Netten SM (2005) Rapid responses of the cupula in the lateral line of ruffe (*Gymnocephalus cernuus*) J Comp Physiol A, 191:393–401

Coombs S, Görner P, Münz H (1989) The mechanosensory lateral line: neurobiology and evolution. Springer, Berlin Heidelberg New York

Coombs, S, Hastings, M, Finneran, JJ (1996) Modeling and measuring lateral line excitation patterns to changing dipole source locations. J Comp Physiol A 178:359–371

Coombs S, Janssen J (1990) Behavioral and neurophysiological assessment of lateral line sensitivity in the mottled sculpin, *Cottus bairdi*. J Comp Physiol A 167:557–567

Coombs S, Janssen J, Webb JF (1988) Diversity of lateral line systems: evolutionary and functional considerations. In: Atema J, Fay RR, Popper AN, Tavolga WN (eds) Sensory biology of aquatic animals. Springer, Berlin Heidelberg New York pp 553–593

Coombs S, Janssen J, Montgomery JC (1992) Functional and evolutionary implications of peripheral diversity in lateral line systems. In: Webster DB, Fay RR, Popper AN (eds) The evolutionary biology of hearing. Springer, Berlin Heidelberg New York, pp 267–294

Coombs S, Montgomery JC (1992) Fibers innervating different parts of the lateral line system of an Antarctic Notothenioid, *Trematomus bernacchii*, have similar frequency responses, despite large variations in the peripheral morphology. Brain Behav Evol 40:217–233

Coombs S, Montgomery JC (1999) The enigmatic lateral line system. In: Fay RR, Popper AN (eds) Comparative hearing: fish and amphibians. Springer, Berlin Heidelberg New York, pp 319–362

Corey DP, Garcia-Anoveros J, Holt JR, Kwan KY, Lin SY, Vollrath MA, Amalfitano A, Cheung EL, Derfler BH, Duggan A, Geleoc GS, Gray PA, Hoffman MP, Rehm HL, Tamasauskas D, Zhang DS (2004) TRPA1 is a candidate for the mechanosensitive transduction channel of vertebrate hair cells. Nature 432:723–730

Denton EJ, Blaxter, JHS (1976) The mechanical relationships between the clupeid swimbladder, inner ear and the lateral line. J Mar Biol Assoc UK 56:787–807

Denton EJ, Gray JAB (1982) The rigidity of fish and patterns of lateral line stimulation. Nature 297:679–681

Denton EJ, Gray JAB (1983) Mechanical factors in the excitation of clupeid lateral lines. Proc R Soc Lond B 218:1–26

Denton EJ, Gray JAB (1988) Mechanical factors in the excitation of the lateral line of fishes. In: Atema J, Fay RR, Popper AN, Tavolga WN (eds) Sensory biology of aquatic animals. Springer, Berlin Heidelberg New York, pp 595–617

Denton EJ, Gray JAB (1989) Some observations on the forces acting on neuromasts in fish lateral line canals In: Coombs S, Görner P, Münz H (eds) The mechanosensory lateral line: neurobiology and evolution. Springer, Berlin Heidelberg New York, pp 229–246

Dijkgraaf S (1963) The functioning and significance of the lateral-line organs. Biol Rev 38:51–105

Elepfandt A (1982) Accuracy of taxis response to water waves in the clawed toad (*Xenopus laevis* Daudin) with intact or with lesioned lateral line system. J Comp Physiol 148:535–545

Engelmann J, Hanke W, Mogdans J, Bleckmann H (2000) Hydrodynamic stimuli and the fish lateral line. Nature 408:51–52

Engelmann J, Hanke W, Bleckmann H (2002) Lateral line reception in still- and running water. J Comp Physiol A 188:513–526

Enger PS, Kalmijn AJ, Sand O (1989) Behavioral investigations on the functions of the lateral line and inner ear in predation. In: Coombs S, Görner P, Münz H (eds) The mechanosensory lateral line: neurobiology and evolution. Springer, Berlin Heidelberg New York, pp 575–587

Flock Å (1965) Electron microscopic and electro-physiological studies on the lateral line organ. Acta Oto-Laryngol Suppl 199:1–90

Géléoc GS, Lennan GW, Richardson GP, Kros CJ (1997) A quantitative comparison of mechanoelectrical transduction in vestibular and auditory hair cells of neonatal mice. Proc R Soc Lond B 1997 264:611–621

Görner P (1963) Untersuchungen zur Morphologie und Electrophysiologie des Seitenlinienorgans vom Krallenfrosch (*Xenopus laevis* Daudin). Z Vergl Physiol 47:316–338

Harris GG, van Bergeijk WA (1962) Evidence that the lateral line organ responds to near field displacements of sound sources in water. J Acoust Soc Am 34:1831–1841.

Harris GG, Frishkopf LS, Flock Å (1970) Receptor potentials from hair cells of the lateral line. Science 167:76–79

Hassan ES (1986) On the discrimination of spatial intervals by the blind cave fish (*Anoptichthys jordani*). J Comp Physiol A 159:701–710.

Hoekstra D, Janssen J (1985) Non-visual feeding behavior of the mottled sculpin, *Cottus bairdi*, in Lake Michigan. Env Biol Fishes 12:111–117

Howard J, Hudspeth AJ (1988) Compliance of the hair bundle associated with gating of mechanoelectrical transduction channels in the bullfrog's saccular hair cell. Neuron 1:189–199

Hudspeth AJ, ChoeY, Mehta AD, Martin P (2000) Putting ion channels to work: Mechanoelectrical transduction, adaptation, and amplification by hair cells. Proc Natl Acad Sci USA 97:11765–11772

Jielof R, Spoor A, de Vries H (1952) The microphonic activity of the lateral line. J Physiol 116:137–157

Kalmijn AJ (1988) Hydrodynamic and acoustic field detection. In: Atema J, Fay RR, Popper AN, Tavolga WN (eds) Sensory biology of aquatic animals Springer, Berlin Heidelberg New York, pp 83–130

Kalmijn AJ (1989) Functional evolution of lateral line and inner ear sensory systems. In: Coombs S, Görner P, Münz H (eds) The mechanosensory lateral line: Neurobiology and evolution. Springer, Berlin Heidelberg New York, pp 187–215

Karlsen HE, Sand O (1987) Selective and reversible blocking of the lateral line in freshwater fish. J Exp Biol 133:249–263
Kelly JP, van Netten SM (1991) Topography and mechanics of the cupula in the fish lateral line. Variations of cupular structure and composition in three dimensions. J Morph 207:23–36
Kroese ABA, van der Zalm JM, van den Bercken J (1978) Frequency response of the lateral line organ of Xenopus laevis. Pfluegers Arch 375:167–175
Kroese ABA, van den Bercken J. (1980) Dual action of ototoxic antibiotics on sensory hair cells. Nature 283:395–397
Kroese ABA, van den Bercken J (1982) Effects of ototoxic antibiotics on sensory hair cell functioning. Hearing Res 6:183–97
Kroese ABA, van Netten SM (1989) Sensory transduction in lateral line sensory hair cells. In: Coombs S, Görner P, Münz H (eds) The mechanosensory lateral line: Neurobiology and evolution. Springer, Berlin Heidelberg New York, pp 265–284
Kroese ABA, Schellart NAM (1992) Velocity- and acceleration sensitive units in the trunk lateral line of the trout. J Neurophysiol 68:2212–2221
Kuiper JW (1956) The microphonic effect of the lateral line organ. PhD thesis, University of Groningen, The Netherlands
Lamb H (1932) Hydrodynamics. Reprint 6th edn. Dover, New- York
Landau LD, Lifshitz EM (1980) Statistical physics, Part 1. 3rd edn. Pergamon Press, Oxford
Landau LD, Lifshitz EM (1987) Fluid mechanics. 2nd edn. Pergamon Press, Oxford
Leydig F (1850) Ueber die Schleimkanäle der Knochenfische. Müll Arch Anat Physiol 170–181
Liff HJ, Shamres S (1972) Structure and motion of cupulae of lateral line organs in *Necturus maculosu*s III. A technique for measuring the motion of free-standing lateral line cupulae. Q Progr Rep Res Lab Electr MIT 104:332–336
van Maarseveen JThPW (1994) Mechanophysiological investigation on the lateral line of the ruffe. PhD Thesis, University of Groningen, The Netherlands
Markin VS, Hudspeth AJ (1995) Gating-spring models of mechano-electrical transduction by hair cells of the internal ear. Annu Rev Biophys Biomol Struct 24:59–83
Martin P, Jülicher F, Hudspeth AJ (2003) The contribution of transduction channels and adaptation motors to the the hair cell's active process. In: Gummer AW (ed) Biophysics of the cochlea: From molecules to models. World Scientific, Singapore pp 3–15
Mathews J, Walker RL (1970) Mathematical methods of physics. Benjamin, New York
Montgomery JC, Baker CF, Carton AG (1997) The lateral line can mediate rheotaxis in fish. Nature 389:960–963
Montgomery JC, Coombs S, Janssen J (1994) Form and function relationships in lateral line systems: Comparative data from six species of Antarctic notothenioid fish. Brain Behav Evol 44:299–306
Montgomery JC, Macdonald JA (1987) Sensory tuning of lateral line receptors in Antartic fish to the movements of planktonic prey. Science 235:195–196
Münz H (1985) Single unit activity in the peripheral lateral line system of the cichlid fish *Sarotherodon niloticus* L. J Comp Physiol A 157:555–568
Münz H (1989) Functional organization of the lateral line periphery. In: Coombs S, Görner P, Münz H (eds) The mechanosensory lateral line: Neurobiology and evolution. New York: Springer, Berlin Heidelberg New York pp. 285–297
van Netten SM (1988) Laser interferometer microscope for the measurement of nanometer vibrational displacements of a light scattering microscopic object. J Acoust Soc Am 83:1667–1674
van Netten SM (1991) Hydrodynamics of the excitation of the cupula in the fish canal lateral line. J Acoust Soc Am 89:310–319
van Netten SM, Dinklo T, Marcotti W, Kros CJ (2003) Channel gating forces govern accuracy of mechano-electrical transduction in hair cells. Proc Natl Acad Sci USA 100:15510–15515
van Netten SM, Karlsson KJ, Khanna SM and Flock Å (1994) Effects of quinine on the mechanical frequency response of the cupula in the fish lateral line. Hearing Res 73:223–230
van Netten SM, Khanna SM (1994) Stiffness changes of the cupula associated with the mechanics of hair cells in the fish lateral line. Proc Natl Acad Sci USA 91:1549–1553
van Netten SM, Kroese ABA (1987) Laser interferometric measurements on the dynamic behavior of the cupula in the fish lateral line. Hearing Res 29: 55–61.
van Netten SM, Kroese ABA (1989) Dynamic behavior and micromechanical properties of the cupula. In: Coombs S, Görner P, Münz H (eds) The mechanosensory lateral line: Neurobiology and evolution. New York: Springer, Berlin Heidelberg New York, pp 247–263
van Netten SM., Kros CJ (2000). Gating energies and forces of the mammalian hair cell transducer channel and related hair bundle mechanics. Proc R Soc Lond B Biol Sci 267:1915–1923
van Netten SM, van Maarseveen JThPW (1994) Mechanophysiological properties of the supraorbital lateral line canal in ruffe (*Acerina Cernua* L.) Proc R Soc Lond B 256:239–246
van Netten SM (1997) Hair cell mechano-transduction: Its influence on the gross mechanical characteristics of a hair cell organ, Biophys Chem 68:43–52
Nicolson T, Rusch A, Friedrich RW, Granato M, Ruppersberg JP, Nusslein-Volhard C (1998) Genetic analysis of vertebrate sensory hair cell mechanosensation: the zebrafish circler mutants. Neuron 20:271–83
Northcutt RG (1989) The phylogenetic distribution and innervation of craniate mechanoreceptive lateral lines. In: Coombs S, Görner P, Münz H (eds) The mechanosensory lateral line: Neurobiology and evolution. New York: Springer, Berlin Heidelberg New York, pp 17–78
Olson ES (1998) Observing middle and inner ear mechanics with novel intracochlear pressure sensors. J Acoust Soc Am 103:3445–3463
Partridge BL, Pitcher TJ (1980) The sensory basis of fish schools: relative roles of lateral line and vision. J Comp Phys 135:315–325
Ricci AJ, Crawford AC, Fettiplace R. (2002) Mechanisms of active hair bundle motion in auditory hair cells. J Neurosci. 22:44–52.
Russell IJ (1976) Amphibian lateral line receptors. In: Llinas R, Precht W (eds) Frog Neurobiology. Springer, Berlin Heidelberg New York, pp 513–550
Russell IJ, Kossl M, Richardson GP (1992). Nonlinear mechanical responses of mouse cochlear hair bundles. Proc R Soc Lond B Biol Sci 250:217–27
Sand O (1984) Lateral-line systems. In: BolisL, Keynes RD, Maddrell SHP (eds) Comparative physiology of sensory systems. Cambridge University Press, London pp 3–32
Schlichting H (1979) Boundary layer theory. 7th edn. McGraw-Hill, New York
Schulze FE (1861) Über die Nervenendigung in den sogenannten Schleimkanälen der Fische und über entsprechende Organe der durch Kiemen athmenden Amphibien. Arch Anat Physiol Lpz 759–769
Sexl T (1930) Über den von E.G. Richardson entdeckten "Annulareffekt". Z Phys 61:349–362
Sidi S, Friedrich RW, Nicolson T (2003). NompC TRP channel required for vertebrate sensory hair cell mechanotransduction. Science 301:96–99
Söllner C, Rauch GJ, Siemens J, Geisler R, Schuster SC, The Tübingen (2000) Screen Consortium, Müller U, Nicolson T (2004) Mutations in cadherin 23 affect tip links in zebrafish sensory hair cells. Nature 428:955–959
Stokes GG (1851) On the effect of the internal friction of fluids on the motion of pendulums. Trans Camb Phil Soc 9:6–106
Strelioff D, Honrubia V (1978) Neural transduction in *Xenopus Laevis* lateral line system. J Neurophysiol 41:432–444
Tsang PTSK (1997) Laser interferometric flow measurements in the lateral line organ. PhD thesis, University of Groningen, The Netherlands
Tsang PTSK, van Netten SM (1997) Fluid flow profiles measured in the supraorbital lateral line canal of the ruff. In: Lewis ER, Long GR, Lyon RF, Narris PM, C.R. Steele CR, Hecht-Poinar E (eds) Diversity in auditory mechanics. Singapore: World Scientific, pp. 25–31
Webb JF (1989) Developmental constraints and evolution of the lateral line system in teleost fishes. In: Coombs S, Görner P, Münz H (eds)

The mechanosensory lateral line: Neurobiology and evolution. New York: Springer, Berlin Heidelberg New York, pp 79–97
Wiersinga-Post JEC, van Netten SM (1998) Amiloride causes changes in the mechanical properties of hair cell bundles in the fish lateral line similar to those induced by dihydrostreptomycin. Proc R Soc Lond B 265:615–623
Wiersinga-Post JEC, van Netten SM (2000) Temperature dependency of cupular mechanics and hair cell frequency selectivity in the fish canal lateral line organ. J Comp Physiol 186: 949–956
Womersley JR (1955) Method for the calculation of velocity, rate of flow and drag in arteries when the pressure gradient is known. J Physiol 127:553–563
Wubbels RJ (1992) Afferent respons of a head canal neuromast of the Ruff (*Acerina cernua*) lateral line. Comp Biochem Physiol 102A: 19–26